Yuji Hasegawa

TECHNISCHE UNIVERSITÄT WIEN
Vienna University of Technology

Diplomarbeit

Spin-Rotation-Coupling in Neutron Polarimetry

ausgeführt am

Atominstitut

der Technischen Universität Wien

unter der Anleitung von

Assistant Prof. Dipl.-Ing. Dr. Yuji Hasegawa

durch

Bülent Demirel

Datum

Bülent Demirel

Abstract

The study of measurable effects in non-inertial reference frames in quantum physics has been paid a great deal of attention to in recent decades, since one must inevitably deal with the effects of gravity and rotation in microscopic dimensions for a better understanding of nature. In this field neutron physics has played a prominent role in the past, as the *COW (Colella Overhauser Werner) - experiment* and the measurement of the *Sagnac* effect have impressively demonstrated. In 1988, Mashhoon [Phys. Rev. Lett. **61**, 2639 (1988)] predicted a new relativistic quantum mechanical effect, i.e. a coupling of spin with the angular velocity of a rotating reference system. Following the prediction, the spin-rotation interaction has been successfully derived from the Dirac theory, a concrete measurement however is still missing. The first proposal in this regard included a measurement via neutron-interferometry. In this thesis an experimental study of spin-rotation coupling is described. The original idea of the experiment by Mashhoon has been adapted to a set-up using a neutron polarimeter. This measurement method has advantages over neutron-interferometry, in particular because of higher insensitivity to ambient disturbances. Experimental parameters, such as dimensions of various coils for spin-manipulation, were determined and a set-up was constructed. In the first measurement, problems with stray fields were encountered. In order to avoid them, two DC-coils were added to the original polarimeter arrangement. The final results show that a phase shift due to an interaction of angular velocity of a rotating magnetic field and spin could be measured successfully and agree well with theoretical predictions.

Kurzfassung

Der Untersuchung messbarer Effekte in Nicht-Inertialsystemen in der Quantenphysik wurde in den letzten Jahrzenten eine große Aufmerksamkeit geschenkt, da man für ein besseres Verständnis der Natur sich auch zwangsläufig mit den Einflüssen von Gravitation und Rotationen in mikroskopischen Dimensionen auseinandersetzen muss. Die Neutronenphysik stellte in der Vergangenheit diesbezüglich eine herausragende Rolle dar, wie das *COW (Colella Overhauser Werner) - Experiment* und die Messung des *Sagnac* Effekts eindrucksvoll bewiesen haben. Im Jahr 1988 sagte Mashhoon [Phys. Rev. Lett. **61**, 2639 (1988)] einen neuen relativistisch-quantenmechanischen Effekt voraus, die Kopplung von Spin mit der Winkelgeschwindigkeit eines rotierenden Bezugssystems. Nach der Vorhersage dieser Wechselwirkung gelang auch eine Herleitung dieser Spin-Rotationskopplung aus der Dirac-Theorie, eine konkrete Messung blieb bis jetzt jedoch aus. Der erste Vorschlag diesbezüglich umfasste eine Messung mittels der Neutroneninterferometrie. In dieser Diplomarbeit wird eine experimentelle Erforschung dieser Spin-Rotationskopplung durchgeführt. Dabei wurde die ursprüngliche Grundidee jenes Experiments an das Konzept eines Neutronenpolarimeters angepasst. Diese Messmethode hat Vorteile gegenüber der Neutroneninterferometrie auf Grund geringer Empfindlichkeit gegenüber äußeren Störungen. Experimentelle Parameter, wie die Dimensionen verschiedener Spulen zur Spin-Manipulation, wurden bestimmt und ein Versuchsaufbau wurde konstruiert. In der ersten Messung ergaben sich Probleme mit Streufeldern. Um diese zu vermeiden, wurden zwei DC-Spulen der ursprünglichen Polarimeteranordnung beigefügt. Die Endresultate zeigen, dass eine Phasenverschiebung auf Grund der Wechselwirkung der Winkelgeschwindigkeit eines rotierenden Magnetfeldes und des Spins gemessen werden konnte und in guter Übereinstimmung mit der Theorie sind.

Acknowledgements

First of all I would like to express my deepest appreciation to my supervisor Yuji Hasegawa for giving me the opportunity to participate in this experiment and supporting me throughout the entire project. I am grateful to him for his expert, his patient guidance and his thoughtful comments.

Besides, I would like to thank Stephan Sponar, who contributed tremendously to this project with his assistance. In addition, a thank you to my fellow students, who would always lend a sympathetic ear to my problems. I would also like to acknowledge the services of the workshop at the *Institute of Atomic and Subatomic Physics*.

I'm particularly indebted to my family. This thesis is dedicated to my parents and my sister, who supported me all the time and helped me reaching my personal goals.

Notations

The following conventions are used in this thesis:

Latin indices i, j, k run from 1-3 and stand for the space components.
Greek indices run from 0-4 and stand for the spacetime components. *Lorentz indices*, *non-coordinate indices* are given by the first four letters of the Greek alphabet α, β, γ, δ, whereas *general spacetime*, *coordinate indices* are given by μ, ν, σ, ρ.
The canonical form of the metric tensor in flat spacetime is $\eta_{\alpha\beta} = diag(1, -\mathbb{1}_3)$. The spacetime metric tensor is denoted as $g_{\mu\nu}$.
Basis vectors are will be given in the form $\hat{\boldsymbol{e}}_{(\mu)}$. Parentheses emphasise that the index labels not components of a single vector, but a collection of vectors.

Contents

1 Introduction

Accelerating frames of reference are essential in physics. Because of gravity and rotation every measurement in a stationary laboratory on Earth takes place in a non-inertial frame in the strict sense. In classical mechanics the description of the equation of motion introduces the well known Coriolis force and the centrifugal force. In the middle of the 19th century the Foucault pendulum has been one of the fascinating observational consequences of the rotational nature of local laboratory frames. About 60 years later Sagnac observed the correlation of angular velocity and the phase-shift of light in a ring interferometer.
Through the development of quantum physics at the beginning of the 20th century, the question of measurable effects of rotations in microscopic dimensions came up. Moreover the discovery of the spin by the Stern Gerlach experiment expanded the idea of rotation by an intrinsic form of angular momentum, the spin of an elemental particle, which is however not a rotation in the 'real' sense. Parallel to the discussions on the wave-particle duality, experiments succeeded in showing the wave nature of elementary particles, for instance the interference of neutrons. In the last few decades the use of neutron waves enabled the verification of a wide spectrum of quantum phenomena, such as the Sagnac effect, the influence of the earth's gravitational potential on the neutron phase, see the *COW (Colella Overhauser Werner)* experiment, or the measurement of the *geometric phase*. It is therefore not surprising that neutrons have been used in many experiments to measure effects in non-inertial frames.
In his study of the description of rotating observers, in 1988 physicist B. Mashhoon predicted a coupling of the intrinsic spin $\mathbf{S}$ with rotation [1], i.e. a term of the form $\mathbf{\Omega} \cdot \mathbf{S}$, by theory. If a particle with respect to an inertial frame and a frame that is in relative rotation to the other by the angular frequency $\mathbf{\Omega}$ is considered, the (classical or quantum-mechanical) Hamilton operators of the respective frames only differ by an angular momentum term $\mathbf{\Omega} \cdot \mathbf{L}$, which is the basis of the well known Sagnac effect [2]. Expanding this concept by performing the appropriate replacement of $\mathbf{L}$ with the total

angular momentum operator $\mathbf{J}$, i.e. $\mathbf{L} \to \mathbf{J} = \mathbf{L} + \mathbf{S}$, would create the aforementioned additional *spin rotation coupling*. The Sagnac term has already been observed in experiments [2]. A derivation from the Dirac theory has further established the existence of this interaction, yet measurements still had to verify the theoretical predictions. There have been some indications of the existence of this effect though [3], [4] and an analogous *helicity-rotation* coupling for photons [5] could be detected.
Ever since the publication of [1] experimental set-ups have been proposed to measure this effect. In 2005 Mashhoon, Kaiser have clearly outlined a neutron interferometer experiment [6], which is the original model for the neutron polarimetry experiment described in this work.

This thesis is devoted to the measurement of the spin-rotation coupling in neutron polarimetry. The aim of the 2. Chapter is to summarize the theoretical foundations that are needed to derive the spin rotation coupling from the Dirac theory, which is the correct relativistic equation to describe spin 1/2 particles. Afterwards a change to the prescription of the Dirac equation in a rotating frame of reference is implemented, where all important terms are introduced. Subsections will then deal with the non relativistic limits and then solve the analogous *Pauli* equation in a rotating magnetic field. Chapter 3 will give a brief overview of the experimental tools and instruments that are needed for the polarimeter set-up. In addition, examples of quantum-mechanical investigations and accomplishments with neutron polarimeter are described. In Chapter 4, the measurement of the spin-rotation coupling is explained. According to preliminary calculations a longer coil is fabricated. First trials show unexpected results and make improvements on the original set-up necessary. In the final section the results are presented and show the verification of the predicted spin-rotation coupling.

2 Theoretical foundations

2.1 Derivation of spin rotation coupling in the Dirac theory

2.1.1 Dirac equation in flat spacetime

The opening of this chapter starts with an opportunity to briefly recall some familiar properties of the Dirac theory, which will be needed to sketch the derivation of the Spin-Rotation coupling $\boldsymbol{\omega} \cdot \mathbf{S}$. Mathematical formulas of the Dirac theory in flat spacetime will be introduced axiomatically without evidence or any efforts to emphasise or prove the relations, giving references to certain terms and equations, that are suspected to be unknown. Major sources for the following relations are [7] and [8].
In the relativistic regime the evolution of a massive particle is given by the Dirac equation

$$i\hbar\frac{\partial}{\partial t}\psi(\mathbf{r},t) = \left[c\sum_{i=1}^{3}\hat{\alpha}_i\hat{p}^i + \hat{\beta}mc^2\right]\psi(\mathbf{r},t)\,, \tag{2.1}$$

where the Dirac Hamiltonian H_D is given by the expression in the square bracket

$$H_D = c\,\hat{\alpha}_i\hat{p}^i + \hat{\beta}mc^2\,, \tag{2.2}$$

where the *Einstein summation convention* has been implemented casually in Eq. (2.2) and will be used from now on. In this representation Eq. (2.1) resembles the typical form of the famous Schrödinger equation

$$i\hbar\frac{\partial}{\partial t}\psi(\mathbf{r},t) = H_D\psi(\mathbf{r},t)\,. \tag{2.3}$$

There are however new elements in Eq. (2.2) that need some explanation. To be more precise the two new components $\hat{\alpha}_i$ and $\hat{\beta}$, that have been introduced, come along with several conditions:

- For the Hamiltonion H_D in Eq. (2.2) to be Hermitian, $\hat{\alpha}_i$ and $\hat{\beta}$ also have to be Hermitian matrices.
- The components $\hat{\alpha}_i$ and $\hat{\beta}$ have to obey the following three mathematical conditions making these elements belong to a certain algebraic structure, i.e. the *Clifford-Algebra*:

$$\hat{\alpha}_i\hat{\alpha}_j + \hat{\alpha}_j\hat{\alpha}_i = \{\hat{\alpha}_i, \hat{\alpha}_j\} = 2\delta_{ij}\mathbb{1} \tag{2.4}$$

$$\hat{\alpha}_i\hat{\beta} + \hat{\beta}\hat{\alpha}_i = \{\hat{\alpha}_i, \hat{\beta}\} = 0 \tag{2.5}$$

$$\hat{\beta}^2 = \mathbb{1}\,. \tag{2.6}$$

For spin-1/2 particles the Eqs. (2.4) - (2.6) require $\hat{\alpha}_i$ and $\hat{\beta}$ to be 4×4 matrices, whose standard representation is given by

$$\hat{\alpha}_i = \begin{pmatrix} 0 & \hat{\sigma}_i \\ \hat{\sigma}_i & 0 \end{pmatrix} \qquad \hat{\beta} = \begin{pmatrix} \mathbb{1}_2 & 0 \\ 0 & -\mathbb{1}_2 \end{pmatrix}, \tag{2.7}$$

where the typical block notation with 2×2 matrices has been used for the identity matrix $\mathbb{1}_2 = \text{diag}(1{,}1)$ and the *Pauli matrices* $\hat{\sigma}_i$, witch are

$$\hat{\sigma}_x = \begin{pmatrix} 0 & 1 \\ 1 & 0 \end{pmatrix} \qquad \hat{\sigma}_y = \begin{pmatrix} 0 & -i \\ i & 0 \end{pmatrix} \qquad \hat{\sigma}_z = \begin{pmatrix} 1 & 0 \\ 0 & -1 \end{pmatrix}. \tag{2.8}$$

The *Hermicity* and the anti-commutation rules are the only constraints on $\hat{\alpha}_i$ and $\hat{\beta}$. The representation of the matrices $\hat{\alpha}_i$ and $\hat{\beta}$ is unique up to a unitary equivalence $\hat{\alpha}_i \to \hat{U}\hat{\alpha}_i\hat{U}^{-1}$ and $\hat{\beta} \to \hat{U}\hat{\beta}\hat{U}^{-1}$ with $\hat{U}\hat{U}^\dagger = \mathbb{1}$.
As a consequence of the matrix property of $\hat{\alpha}_i$, $\hat{\beta}$ the wave-function $\psi(\mathbf{r}, t)$ becomes a vector of 4 wave functions, which is called *spinor*

$$\psi(\mathbf{r},t) = \begin{pmatrix} \psi_1(\mathbf{r},t) \\ \psi_2(\mathbf{r},t) \\ \psi_3(\mathbf{r},t) \\ \psi_4(\mathbf{r},t) \end{pmatrix} . \tag{2.9}$$

Lorentz Covariant representation of the Dirac equation

In a majority of cases the Dirac equation for a free particle is given not in the form (2.1) but in an equivalent, yet more obvious, *Lorentz covariant form*

$$[i\hbar\hat{\gamma}^\alpha\partial_\alpha - mc]\,\psi(\mathbf{x}) = 0\,, \tag{2.10}$$

where the anti-commutation relations Eqs. (2.4) - (2.6) now reads as

$$\{\hat{\gamma}^\alpha, \hat{\gamma}^\beta\} = 2\eta^{\alpha\beta}\mathbb{1} \tag{2.11}$$

and the new *gamma matrices* $\hat{\gamma}^\alpha = (\hat{\gamma}^0\,,\,\hat{\gamma}^i)^T$, also called *Dirac matrices*, are related to $\hat{\alpha}_i$ and $\hat{\beta}$ by

$$\hat{\gamma}^0 = \hat{\beta} \qquad \hat{\gamma}^i = \hat{\beta}\hat{\alpha}_i\,. \tag{2.12}$$

The gamma matrices $\hat{\gamma}^\alpha$ are unitary, but for $\alpha \neq 0$ not Hermitian: $\hat{\gamma}^i = -(\hat{\gamma}^i)^\dagger$. This property is called *skew-Hermitian*. With the relations above the Hamiltonian Eq. (2.2) can also be written in terms of the gamma matrices

$$H_D = c\hat{\gamma}^0\hat{\gamma}^i\hat{p}_i + \hat{\gamma}^0 mc^2\,. \tag{2.13}$$

At this point the definition of *covariance* should be clarified.
The meaning of *general covariance* refers to physical laws, which are invariant under arbitrary differentiable coordinate transformations. A mathematical description that is independent of charts can be obtains by employing tensorial quantities, that under a change of coordinates obey the general tensor transformation law

$$T^{\mu_1'\cdots\mu_m'}{}_{\nu_1'\cdots\nu_n'} = \frac{\partial x^{\mu_1'}}{\partial x^{\mu_1}}\cdots\frac{\partial x^{\mu_m'}}{\partial x^{\mu_m}}\,\frac{\partial x^{\nu_1}}{\partial x^{\nu_1'}}\cdots\frac{\partial x^{\nu_n}}{\partial x^{\nu_n'}}\,T^{\mu_1\cdots\mu_m}{}_{\nu_1\cdots\nu_n}\,. \tag{2.14}$$

For example, the components of a vector V^{μ} transforms like

$$V^{\mu'} = \frac{\partial x^{\mu'}}{\partial x^{\mu}} V^{\mu} \,. \tag{2.15}$$

For a mixed tensor of rank 2, Eq. (2.14) yields

$$F^{\mu'}{}_{\nu'} = \frac{\partial x^{\mu'}}{\partial x^{\mu}} \frac{\partial x^{\nu}}{\partial x^{\nu'}} F^{\mu}{}_{\nu} \,. \tag{2.16}$$

These objects transform under general coordinate transformations. *Lorentz covariance* is a special kind of linear coordinate transformation in flat spacetime, that only calls for invariance under a global *Lorentz transformation*

$$V^{\alpha'} = \Lambda^{\alpha'}{}_{\alpha} V^{\alpha} \,, \tag{2.17}$$

where the $\hat{\Lambda}$'s also satisfy the relation

$$\eta_{\alpha\beta} = \Lambda^{\alpha'}{}_{\alpha} \Lambda^{\beta'}{}_{\beta} \eta_{\alpha'\beta'} \,. \tag{2.18}$$

Hence the indices of a tensor, that is covariant under Lorentz transformation, is given by

$$T^{\alpha'_1 \cdots \alpha'_m}{}_{\beta'_1 \cdots \beta'_n} = \Lambda^{\alpha'_1}{}_{\alpha_1} \cdots \Lambda^{\alpha'_m}{}_{\alpha_m} \Lambda_{\beta'_1}{}^{\beta_1} \cdots \Lambda_{\beta'_n}{}^{\beta_n} T^{\alpha_1 \cdots \alpha_m}{}_{\beta_1 \cdots \beta_n} \,, \tag{2.19}$$

where $\Lambda_{\beta'}{}^{\beta} \equiv (\Lambda^{-1})^{\beta'}{}_{\beta}$, i.e. the inverse of the Lorentz transformation. If the Dirac equation is Lorentz covariant, then results of this theory are valid in all frames in flat spacetime. A set of these spacetime independent matrices $\hat{\Lambda}$ form the *Lorentz group* under matrix multiplication O(3,1). Employing the following two conditions

$$det(\Lambda) = +1 \qquad \Lambda^{0}{}_{0} \geq 1 \,, \tag{2.20}$$

yields the *proper*, *orthochronous* Lorentz subgroup $SO^{+}(3,1)$, which is the Lorentz group that is usually being referred to.
Since Eq. (2.1) is conform with quantum mechanics and special relativity, the question remains how spinors change under a Lorentz transformation. One has to distinguish between *Minkowski-space* and *4-spinors*, that are elements of a complex vector space.

For this purpose a matrix $\hat{S}(\hat{\Lambda})$ is applied to the spinor, which takes $\psi'(x^{\mu'})$ (notice that the prime is not just over the index) to $\psi(x^{\mu})$ under a Lorentz transformation

$$\psi'(\mathbf{x}') = \hat{S}(\hat{\Lambda})\psi(\mathbf{x})\,. \tag{2.21}$$

Inserting this ansatz into Eq. (2.10) in the primed reference frame, i.e. spin and coordinate transformed representation, yields

$$\hat{S}(\hat{\Lambda})\,\hat{\gamma}^{\alpha}\,\Lambda^{\alpha'}{}_{\alpha}\hat{S}^{-1}(\hat{\Lambda}) = \hat{\gamma}^{\alpha'}\,. \tag{2.22}$$

The inclusion of Lorentz covariant spin transformation has led to the necessary transformation (2.22), that connects two distinct sets of Dirac - matrices, of which both satisfy the Clifford relations. The Lorentz covariance of Eq. (2.10) is "usually approached by keeping the same representation of the $\hat{\gamma}$ matrices in the Lorentz transformed coordinate system so that the burden of the transformation is thrown on the wave function by means of an equivalence transformation" [9]. As an aside, in mathematical jargon spinors transform according to the *covering group* SL(2; $\mathbb{C}$) and there exists a homomorphism from $SL(2, \mathbb{C})$ to the Lorentz group $SO^{+}(1,3)$.
An explicit representation for $\hat{S}$ can be determined by an infinitesimal proper Lorentz transformation

$$\Lambda^{\alpha}{}_{\beta} = \delta^{\alpha}{}_{\beta} + \epsilon^{\alpha}{}_{\beta}\,, \tag{2.23}$$

where $\epsilon_{\alpha\beta} = -\epsilon_{\beta\alpha}$ is antisymmetric. Without proof the form of $\hat{S}$ for finite Lorentz transformation in spinor space is given by [10]

$$S(\hat{\Lambda}) = exp\left(i\,\Sigma_{\alpha\beta}\epsilon^{\alpha\beta}\right)\,, \tag{2.24}$$

where $\Sigma_{\alpha\beta}$ are the generators of the Lorentz group and can be expressed in terms of the gamma matrices as

$$\Sigma_{\alpha\beta} = -\frac{i}{8}\left[\gamma^{\alpha}, \gamma^{\beta}\right]\,. \tag{2.25}$$

The information so far is standard in relativistic quantum mechanic and has been implemented with forethought of the sections to come.

2.1.2 Dirac equation in curved spacetime

In the last section it has been stressed that the Dirac equation is Lorentz covariant, thus expresses the correct transformation between inertial observers. However, to describe accelerating particles mathematically, e.g. particles in a rotating frame, in the relativistic aspect one has to make modifications on the theory. A generally covariant equation is needed, which transforms like a tensor according to Eq. (2.14) and which differentiates the Dirac spinor in curved spacetime correctly. The solution of this problem will be given right after the following necessary preliminary subsection, which is designed to only comprise the most rudimentary explanation of important terms.

The 'frame'work

Often it is required to decompose a vector using some particular coordinate system, that can not only be rectangular but also curvilinear. Common examples of curvilinear coordinates are the polar coordinate system in 2 dimensions or cylindrical and spherical coordinate systems in 3D. In general coordinate lines can also run like in Fig. 2.1, which illustrates a few concepts of curvilinear coordinates. The upcoming content has been extracted primarily form [11] and [12].
The number of coordinate lines (see dashed lines) equals the dimension of the space viewed. In flat spacetime one could define now a globally orthogonal basis. The *basis vectors* in curved spacetime at a specific position, which is indicated by the black vectors in Fig. (2.1), are given only locally by the tangent vectors to the coordinate lines

$$\hat{\boldsymbol{e}}_{(\mu)} = \partial_{(\mu)} \,. \tag{2.26}$$

This is the 'natural' differential basis that spans the tangent space T_p at a point p. A basis like this, that is derived from coordinate lines, is called a *holonomic basis* or *coordinate basis*. Any vector $\mathbf{V} \in T_p$ is therefore given by a linear combination of the $\partial_{(\mu)}$

$$\mathbf{V} = V^{\mu}\hat{\boldsymbol{e}}_{(\mu)} = V^{\mu}\partial_{(\mu)} \,. \tag{2.27}$$

In finite dimensions there exists another associated *dual vector space* V^* of equal dimension. A local *cobasis* in a cotangent space T_p^* is given by the gradients of the coordinate

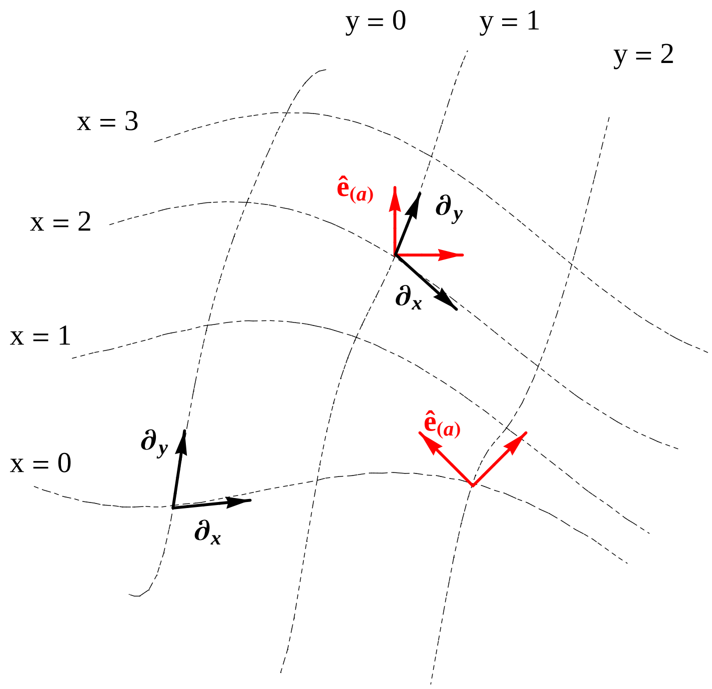

Figure 2.1: Curvilinear chart on a two-dimensional manifold. Black vector are tangents to the coordinate lines and depict the *coordinate basis*. The red vectors are a random basis, known as *tetrad*.

functions

$$\hat{\boldsymbol{\theta}}^{(\mu)} = dx^{(\mu)} \tag{2.28}$$

and a *covector*, also called *dual vector* or *one-form*, can be decomposed as

$$\boldsymbol{\omega} = \omega_\mu \hat{\boldsymbol{\theta}}^{(\mu)} = \omega_\mu dx^{(\mu)} \,. \tag{2.29}$$

The tensor product of the basis and cobasis gives the orthonormality relation

$$\hat{\boldsymbol{e}}_{(\mu)} \otimes \hat{\boldsymbol{\theta}}^{(\nu)} = \delta^\nu_\mu \,. \tag{2.30}$$

With the dual vector space introduced, a linear map from the original vector space to the space of real numbers $V \times V^* \to \mathbb{R}$, can be given by

$$\begin{aligned}\boldsymbol{\omega}(\mathbf{V}) &= \omega_\mu V^\nu \hat{\boldsymbol{e}}_{(\mu)} \hat{\boldsymbol{\theta}}^{(\nu)} \\ &= \omega_\mu V^\nu \delta^\mu_\nu \\ &= \omega_\mu V^\mu \in \mathbb{R}\,.\end{aligned} \tag{2.31}$$

Since these results cannot depend on the coordinate system used, it is possible to choose a different basis, preferably an orthonormal one (which must have the the appropriate signature of the manifold that is worked on). The red vectors $\hat{\boldsymbol{e}}_{(\alpha)}$ in Fig. (2.1) illustrate two bases at two points on the manifold. In reference to the definition above, these bases are called *non-holonomic basis* or *non-coordinate basis* and one particular set of basis is known as *tetrad* or *n-Bein*.

Unlike a coordinate basis, tetrads are independent of a coordinate system, which will, in analogy to flat spacetime indices, be indicated by the first four Greek letters α, β, γ, δ . It is now possible to write the position-dependent coordinate basis as a linear combination of the tetrad

$$\hat{\boldsymbol{e}}_{(\mu)}(\mathbf{x}) = E_\mu{}^\alpha(\mathbf{x})\, \hat{\boldsymbol{e}}_{(\alpha)}\,, \tag{2.32}$$

where $E_\mu{}^\alpha(\mathbf{x})$ is called *vierbein field*, which is a $n \times n$ invertible matrix. The last fact enables the representation of the tetrad in terms of the coordinate basis

$$\hat{\boldsymbol{e}}_{(\alpha)} = E^\mu{}_\alpha(\mathbf{x})\, \hat{\boldsymbol{e}}_{(\mu)}(\mathbf{x}) \tag{2.33}$$

and orthonormality conditions read as

$$E^\mu{}_\alpha(\mathbf{x}) E_\nu{}^\alpha(\mathbf{x}) = \delta^\mu_\nu \qquad E_\mu{}^\alpha(\mathbf{x}) E^\mu{}_\beta(\mathbf{x}) = \delta^\alpha_\beta\,. \tag{2.34}$$

It is favourable for the tetrad to be orthonormal, in which case the metric tensor can be written in the *canonical form* $\eta_{\alpha\beta}$, so that the inner product can be expressed as

$$g\left(\hat{\boldsymbol{e}}_{(\alpha)}, \hat{\boldsymbol{e}}_{(\beta)}\right) = \eta_{\alpha\beta}\,. \tag{2.35}$$

Using Eq. (2.33), this relation in terms of the *vierbein fields* yields

$$g_{\mu\nu}(\mathbf{x}) E^\mu{}_\alpha(\mathbf{x})\, E^\nu{}_\beta(\mathbf{x}) = \eta_{\alpha\beta}\,. \tag{2.36}$$

Naturally, there is a *non-coordinate dual basis* in the cotangent space T_p^*, where (2.30) is analogously defined as

$$\hat{\boldsymbol{\theta}}^{(\alpha)} \otimes \hat{\boldsymbol{e}}_{(\beta)} = \delta^{\alpha}_{\beta} \,, \tag{2.37}$$

just as the Eqs. (2.32), (2.33) change to

$$\hat{\boldsymbol{e}}^{(\mu)}(\mathbf{x}) = E^{\mu}{}_{\alpha}(\mathbf{x})\,\hat{\boldsymbol{e}}^{(\alpha)} \qquad \hat{\boldsymbol{e}}^{(\alpha)} = E_{\mu}{}^{\alpha}(\mathbf{x})\,\hat{\boldsymbol{e}}^{(\mu)}(\mathbf{x})\,. \tag{2.38}$$

Recapitulating the previous definitions, the important concept to be remembered is that there exists an 'inherent basis', that is a set of vectors derived from the mesh of coordinate lines, and an arbitrary 'laboratory frame'. These bases can be mutually related to each other by introducing the *vierbein field*. Same goes for the dual basis. One important property of this *vierbein field* can be seen by the representation of a vector in the two distinct bases

$$\mathbf{V} = V^{\mu}\hat{\boldsymbol{e}}_{(\mu)} = V^{\alpha}\hat{\boldsymbol{e}}_{(\alpha)}\,. \tag{2.39}$$

This indicates that the vierbein field makes it possible to switch between the bases as well as the sets of indices

$$V^{\alpha} = E_{\mu}{}^{\alpha}(\mathbf{x})\,V^{\mu} \qquad V^{\mu} = E^{\mu}{}_{\alpha}(\mathbf{x})\,V^{\mu}\,, \tag{2.40}$$

a method, that can be easily expanded to tensors with mixed indices of arbitrary rank (see (2.44)). The *Minkowski metric* $\eta_{\alpha\beta}$ and the general metric tensor $g_{\mu\nu}$ belong to their respective index and can be used to lower and raise indices, for example

$$E_{\mu}{}^{\alpha}(\mathbf{x}) = g_{\mu\nu}(\mathbf{x})\,\eta^{\alpha\beta}\,E^{\nu}{}_{\beta}(\mathbf{x})\,. \tag{2.41}$$

The next point to settle is to define a transformation of the tetrads 'among each other'. This is achieved by a *local Lorentz transformation*

$$\hat{\boldsymbol{e}}_{(\alpha')} = \Lambda^{\alpha}{}_{\alpha'}(\mathbf{x})\,\hat{\boldsymbol{e}}_{(\alpha)}\,, \tag{2.42}$$

with

$$\eta_{\alpha'\beta'} = \Lambda_{\alpha'}{}^{\alpha}\Lambda_{\beta'}{}^{\beta}\eta_{\alpha\beta}\,. \tag{2.43}$$

With these matrices $\Lambda^{\alpha}{}_{\alpha'}(\mathbf{x})$, which depend on spacetime, Lorentz transformation can now be locally applied in all frames at every point in spacetime. The *general coordinate transformations* of a mixed (2,2) tensor can be written as

$$T^{\alpha'\mu'}{}_{\beta'\nu'} = \Lambda^{\alpha'}{}_{\alpha}(\mathbf{x})\,\frac{\partial x^{\mu'}}{\partial x^{\mu}}\,\Lambda_{\beta'}{}^{\beta}(\mathbf{x})\,\frac{\partial x^{\nu}}{\partial x^{\nu'}}\,T^{\alpha\mu}{}_{\beta\nu}\,. \tag{2.44}$$

Before introducing further concepts the commutator of the tetrads shall be shortly examined here. Unlike in the coordinate base

$$[\hat{\boldsymbol{e}}_{(\mu)}, \hat{\boldsymbol{e}}_{(\nu)}] = [\partial_{(\mu)}, \partial_{(\mu)}] = 0\,, \tag{2.45}$$

the tetrad components do not commute, instead they give rise to the *'commutation constants'* $C^{\gamma}{}_{\alpha\beta}$ [13]

$$\begin{aligned} [\hat{\boldsymbol{e}}_{(\alpha)}, \hat{\boldsymbol{e}}_{(\beta)}] &\overset{(2.33)}{=} \left[E^{\mu}{}_{\alpha}(\mathbf{x})\,\partial_{(\mu)}, E^{\nu}{}_{\beta}(\mathbf{x})\,\partial_{(\nu)}\right] \\ &= E^{\mu}{}_{\alpha}\frac{\partial E^{\nu}{}_{\beta}}{\partial x^{\mu}}\frac{\partial}{\partial x^{\nu}} - E^{\nu}{}_{\beta}\frac{\partial E^{\mu}{}_{\alpha}}{\partial x^{\nu}}\frac{\partial}{\partial x^{\nu}} \equiv C^{\gamma}{}_{\alpha\beta}\hat{\boldsymbol{e}}_{(\gamma)}\,. \end{aligned} \tag{2.46}$$

This equation makes the coefficient constants $C^{\gamma}{}_{\alpha\beta}$ depend only on the tetrad used. In general they will not vanish, but pretty soon they will be of good use.

Connections

The requirement for modifications on the Dirac theory in curved spacetime shall be made apparent by the following point. In flat spacetime tensorial objects are subjected to the transformation Eq. (2.19) and it has been implied, that spinor representations are defined in relation to the double cover of the Lorentz group. To describe a physical law in curved spacetime in all frames equivalently, one uses tensors satisfying the general tensor transform Eq. (2.14), where a set of these tensor transformation matrices represent elements of the general linear group $GL(4,\mathbb{R})$. However, this group has no 'multi-

valued representation'. For a finite-dimensional spinorial representation a restriction of $GL(4,\mathbb{R})$ onto the orthogonal subgroup $SO^{+}(1,3)$ is needed [14].
To put it briefly, spinors in curved spacetime are usually defined relative to a locally Minkowski frame. The piece that needs to be added to the theory is the construct of a *connection*, a mathematical instrument to correctly compare one local geometry with another one at another point of the manifold and relate them correctly.
Writing the *Lorentz covariant* Dirac equation once more

$$[i\hbar\hat{\gamma}^{\alpha}\partial_{\alpha} - mc]\,\psi(\mathbf{x}) = 0\,, \tag{2.10}$$

the first modification sought is a change of the Lorentz tensors with generally covariant tensors (sometimes known as the principle of general covariance), thus

$$\begin{aligned} \eta_{\alpha\beta} &\to g_{\mu\nu}(\mathbf{x}) \\ \hat{\gamma}^{\alpha} &\to \hat{\gamma}^{\mu}(\mathbf{x}) \\ \partial_{\alpha} &\to \partial_{\mu}(\mathbf{x})\,. \end{aligned} \tag{2.47}$$

The first two relations are fine and give the generalization of the anti-commutation rule

$$\{\hat{\gamma}^{\alpha},\hat{\gamma}^{\beta}\} \overset{(2.40)}{\to} \{\hat{\gamma}^{\mu},\hat{\gamma}^{\nu}\} = 2g^{\mu\nu}\mathbb{1}\,, \tag{2.48}$$

but the partial derivative of a tensor is not generally covariant. For example the transform of the derivative of a *covector* $\partial_{\mu}V_{\nu}$ yields

$$\partial_{\mu'}V_{\nu'} \overset{(2.14)}{=} \left(\frac{\partial x^{\mu}}{\partial x^{\mu'}}\partial_{\mu}\right)\left(\frac{\partial x^{\nu}}{\partial x^{\nu'}}V_{\nu}\right) = \frac{\partial x^{\mu}}{\partial x^{\mu'}}\frac{\partial x^{\nu}}{\partial x^{\nu'}}\partial_{\mu}V_{\nu} + V_{\nu}\frac{\partial^2 x^{\nu}}{\partial x^{\mu'}\partial x^{\nu'}}\,. \tag{2.49}$$

Due to the existence of the second term, clearly this is not a (0,2) tensor. A 'correction' term has to be added to the partial derivative, to account for the change of the vector basis along a direction in curvilinear coordinates

$$\partial_{\mu}\hat{\boldsymbol{e}}_{(\nu)} = \partial_{\mu}\partial_{(\nu)} \equiv \partial_{(\sigma)}(\Gamma_{\mu})^{\sigma}{}_{\nu}\,. \tag{2.50}$$

The matrices $(\Gamma_\mu)^\sigma{}_\nu$ are called the *affine connection* or *connection coefficients*, where the parentheses are usually dropped. With this, the covariant derivative can be obtained from

$$\begin{aligned}\partial_\mu \mathbf{V} &= \partial_\mu(\partial_{(\nu)} V^\nu) = \partial_{(\nu)}\partial_\mu V^\nu + \partial_\mu \partial_{(\nu)} V^\nu \\ &\overset{(2.50)}{=} \partial_{(\nu)}\partial_\mu V^\nu + \partial_{(\sigma)} \Gamma^\sigma_{\mu\nu} V^\nu \\ &= \partial_{(\sigma)} \left(\delta^\sigma_\nu \partial_\mu + \Gamma^\sigma_{\mu\nu}\right) V^\nu \equiv \partial_{(\sigma)} (\nabla_\mu)^\sigma{}_\nu V^\nu \,.\end{aligned} \tag{2.51}$$

Thus the correct change from *Lorentz covariant* to *general covariant* is given by $\partial_\alpha \to \hat{\nabla}_\mu$, where $\hat{\nabla}_\mu$ is an abbreviation of $(\nabla_\mu)^\sigma{}_\nu$. The usual properties of the covariant derivative (not all of them are essential) are [12]:

1. Linearity: $\hat{\nabla}(T + S) = \hat{\nabla}T + \hat{\nabla}S$
2. Leibniz product rule: $\hat{\nabla}(T \otimes S) = (\hat{\nabla}T) \otimes S + T \otimes (\hat{\nabla}S)$
3. Commutation with contractions: $\hat{\nabla}_\mu (T^\lambda{}_{\lambda\rho}) = (\hat{\nabla}T)_\mu{}^\lambda{}_{\lambda\rho}$
4. Reduction to partial derivative for scalars: $\hat{\nabla}_\mu \phi = \partial_\mu \phi$
5. Torsion-freeness : $\Gamma^\sigma_{\mu\nu} = \Gamma^\sigma_{\nu\mu}$
6. Metric compatibility: $\hat{\nabla}_\sigma g_{\mu\nu} = 0 \quad .$

The last point in the list of properties is usually defined, because this fixes a unique affine connection on a manifold, called the *Levi-Civita connection* or *Christoffel symbols*. Point 1-4 also enables to write the covariant derivative of vector and covector components as

$$\begin{aligned}\hat{\nabla}_\mu V^\nu &= \partial_\mu V^\nu + \Gamma^\nu_{\mu\sigma} V^\sigma \\ \hat{\nabla}_\mu \omega_\nu &= \partial_\mu \omega_\nu - \Gamma^\sigma_{\mu\nu} \omega_\sigma\end{aligned} \tag{2.52}$$

or generally the covariant derivative of a tensor with upper and lower indices as

$$\hat{\nabla}_\sigma T^{\mu_1\cdots\mu_m}{}_{\nu_1\cdots\nu_n} = \partial_\sigma T^{\mu_1\cdots\mu_m}{}_{\nu_1\cdots\nu_n} + \Gamma^{\mu_1}_{\sigma\lambda} T^{\lambda\cdots\mu_m}{}_{\nu_1\cdots\nu_n} \cdots - \Gamma^\lambda_{\sigma\nu_1} T^{\mu_1\cdots\mu_m}{}_{\lambda\cdots\nu_n} \cdots \tag{2.53}$$

With this Eq. (2.53), the metric compatibility can be rewritten as

$$\hat{\nabla}_\sigma g_{\mu\nu} = \partial_\sigma g_{\mu\nu} - \Gamma^\rho_{\sigma\mu}\, g_{\mu\rho} - \Gamma^\rho_{\sigma\nu}\, g_{\rho\mu} = 0\,. \tag{2.54}$$

It goes without saying that the *affine connection* and the equations corresponding to it can also be represented in a non coordinate basis. For example Eq. (2.50) changes to [15]:

$$\partial_\mu \hat{\boldsymbol{e}}_{(\alpha)} = \omega^{\beta}_{\mu\alpha} \hat{\boldsymbol{e}}_{(\beta)} \,, \tag{2.55}$$

where $\omega^{\beta}_{\mu\alpha}(\mathbf{x})$ in an orthonormal basis is called *spin connection*, *Lorentz connection* or *Ricci rotation coefficients*. A list of important relations for this *spin connection* shall be given. A comparison to (2.52) shows the close analogy to the definitions

$$\begin{aligned} \hat{\nabla}_\mu V^\alpha &= \partial_\mu V^\alpha + {\omega_\mu}^\alpha{}_\beta V^\beta \\ \hat{\nabla}_\mu V_\alpha &= \partial_\mu V_\alpha - {\omega_\mu}^\beta{}_\alpha V_\beta \,, \end{aligned} \tag{2.56}$$

where the *affine connection* Γ and the *spin connection* ω can be related to each other, if the covariant derivative of a vector is examined in both bases

$$\begin{aligned} \hat{\nabla}\mathbf{X} &= \left(\hat{\nabla}_\mu \hat{\boldsymbol{e}}^{(\mu)} \otimes X^\nu \hat{\boldsymbol{e}}_{(\nu)}\right) = \left(\partial_\mu X^\nu + \Gamma^\mu_{\nu\sigma} X^\sigma\right) \left(\hat{\boldsymbol{e}}^{(\mu)} \otimes \hat{\boldsymbol{e}}_{(\nu)}\right) \\ &= \left(\hat{\nabla}_\mu \hat{\boldsymbol{e}}^{(\mu)} \otimes X^\alpha \hat{\boldsymbol{e}}_{(\alpha)}\right) = \left(\partial_\mu X^\alpha + \omega_{\mu\beta}^{\;\;\alpha} X^\beta\right) \left(\hat{\boldsymbol{e}}^{(\mu)} \otimes \hat{\boldsymbol{e}}_{(\alpha)}\right) \,. \end{aligned} \tag{2.57}$$

Using Eqs. (2.39) and (2.41) for the lower right-hand side reveals

$$\begin{aligned} \Gamma^\sigma_{\mu\nu} &= {E_\alpha}^\sigma \left(\partial_\mu {E^\alpha}_\nu + {\omega_\mu}^\alpha{}_\beta {E^\beta}_\nu\right) \\ {\omega_\mu}^\alpha{}_\beta &= -{E_\beta}^\nu \left(\partial_\mu {E^\alpha}_\nu - \Gamma^\sigma_{\mu\nu} {E^\alpha}_\sigma\right) \,. \end{aligned} \tag{2.58}$$

On the the basis of this, the *tetrad postulate* can be derived, by taking the covariant derivative of the vierbein field

$$\hat{\nabla}_\mu {E^\alpha}_\nu(\mathbf{x}) = \partial_\mu {E^\alpha}_\nu - \Gamma^\sigma_{\mu\nu} {E^\alpha}_\sigma + {\omega_\mu}^\nu{}_\beta {E^\beta}_\nu \overset{(2.58)}{=} 0 \,, \tag{2.59}$$

where the Lorentz index got a *spin connection* term and the general index the *affine connection* term. This relation shows that covariant derivative and the vielbein field commute. The next important relation unfolds from the metric compatibility

$$\hat{\nabla}_\sigma g_{\mu\nu} = 0 \overset{(2.35)}{\rightarrow} \hat{\nabla}_\sigma \eta_{\alpha\beta} = \partial_\sigma \eta_{\alpha\beta} - {\omega_\mu}^\gamma{}_\alpha \eta_{\gamma\beta} - {\omega_\mu}^\gamma{}_\beta \eta_{\alpha\gamma} = 0 \,. \tag{2.60}$$

Thus the connection coefficient is antisymmetric in two indices

$$\omega_{\mu\alpha\beta} = -\omega_{\mu\beta\alpha} \,. \tag{2.61}$$

From the vanishing of the torsion it can be shown that under cyclic permutations of the first equation in (2.58) and using the antisymmetric property of the connection coefficient in the orthonormal basis Eq. (2.61) results in [15]

$$\omega_{\alpha\beta\mu} = -\frac{1}{2}\left(C_{\alpha\beta\mu} + C_{\beta\mu\alpha} - C_{\mu\alpha\beta}\right) \,. \tag{2.62}$$

It shall be mentioned that both, affine and spinor connections, do not transform as tensors, but are build such that the covariant derivatives are tensors. In case of the spin connection local Lorentz invariance imposes additionally that $\hat{\nabla}_\mu \Lambda^{\alpha'}{}_\alpha(\mathbf{x}) = 0$, since

$$\hat{\nabla}_\mu V^{\alpha'} = \hat{\nabla}_\mu(\Lambda^{\alpha'}{}_\alpha V^\alpha) = (\hat{\nabla}_\mu \Lambda^{\alpha'}{}_\alpha) V^\alpha + \Lambda^{\alpha'}{}_\alpha (\hat{\nabla}_\mu V^\alpha) \tag{2.63}$$

is only a tensor if the first term on the right side of the equation equals zero. The vanishing of the covariant derivative of the Lorentz transformation can be used to see how the spin connection transforms

$$\begin{aligned} 0 &= \Lambda_{\beta'}{}^\alpha \left(\hat{\nabla}_\mu \Lambda^{\alpha'}{}_\alpha(\mathbf{x})\right) \\ &= \Lambda_{\beta'}{}^\alpha \left(\partial_\mu \Lambda^{\alpha'}{}_\alpha + \omega_\mu{}^{\alpha'}{}_\gamma \Lambda^\gamma{}_\alpha - \omega_\mu{}^\gamma{}_\alpha \Lambda^{\alpha'}{}_\gamma\right) \,. \end{aligned} \tag{2.64}$$

Since $\Lambda_{\beta'}{}^\alpha \Lambda^\gamma{}_\alpha = \delta^\gamma_{\beta'}$ the inhomogeneous spin connection transformation is

$$\omega_\mu{}^{\alpha'}{}_{\beta'} = \Lambda_{\beta'}{}^\alpha \Lambda^{\alpha'}{}_\gamma \omega_\mu{}^\gamma{}_\alpha - \Lambda_{\beta'}{}^\alpha \partial_\mu \Lambda^{\alpha'}{}_\alpha \,. \tag{2.65}$$

Now that all tools for describing spinor fields and taking their derivatives have been developed, the issue of the Dirac equation in curved spacetime can be tackled (without delving too much into the subject).

Explicit Solution

The following two points will be incorporated to devise a generally covariant representation of the Dirac equation:

1. The spinor field $\psi(\mathbf{x})$ transforms as a scalar under general coordinate transformation and under a local Lorentz transformation as
$$\psi(\mathbf{x}) \to \psi'(\mathbf{x}') = \hat{S}(\hat{\Lambda}(\mathbf{x}))\psi(\mathbf{x})\,. \tag{2.66}$$

2. A local spin transformation is carried out by a covariant derivative with $\hat{B}_\mu(\mathbf{x})$ being the *spin connection field*, thus
$$\tilde{\nabla}_\mu \psi(\mathbf{x}) = (\partial_\mu + \hat{B}_\mu)\psi(\mathbf{x})\,. \tag{2.67}$$

Using the correct *principle of general covariance* the Dirac equation in curved spacetime yields

$$\left[i\hbar\hat{\gamma}^\mu \tilde{\nabla}_\mu - mc\right]\psi(\mathbf{x}) = 0\,, \tag{2.68}$$

with $\gamma^\mu = E_\alpha{}^\mu \hat{\gamma}^\alpha$, where the gamma matrices $\hat{\gamma}^\alpha$ are given by the standard representation Eq. (2.12). Local Lorentz invariance of Eq. (2.68) yields a new transformation property of the field $\hat{B}_\mu(\mathbf{x})$, which can be derived from the requirement [10]

$$\tilde{\nabla}_{\mu'}\hat{S}(\hat{\Lambda}(\mathbf{x}))\psi(\mathbf{x}) = \hat{S}(\hat{\Lambda}(\mathbf{x}))\tilde{\nabla}_\mu \psi(\mathbf{x})\,. \tag{2.69}$$

Evaluating the requirement Eq. (2.69) gives

$$\hat{B}_{\mu'}(\mathbf{x}) = \hat{S}^{-1}(\hat{\Lambda}(\mathbf{x}))B_\mu(\mathbf{x})\hat{S}(\hat{\Lambda}(\mathbf{x})) + \hat{S}^{-1}(\hat{\Lambda}(\mathbf{x}))(\partial_\mu \hat{S}(\hat{\Lambda}(\mathbf{x})))\,. \tag{2.70}$$

Representation invariance under a combined local Lorentz and general coordinate transformation in analogy to invariance for the Dirac equation in flat spacetime [10] also yields

$$\left[i\hbar\hat{\gamma}^\alpha E_\alpha{}^\mu \tilde{\nabla}_\mu - mc\right]\psi(\mathbf{x}) = 0$$

$$= \left[i\hbar\hat{\gamma}^\alpha \left(\frac{\partial x^\mu}{\partial x^{\mu'}}\Lambda^{\alpha'}{}_\alpha E_{\alpha'}{}^{\mu'}\right)\tilde{\nabla}_\mu - mc\right]\hat{S}^{-1}(\hat{\Lambda}(\mathbf{x}))\psi'(\mathbf{x}') = 0$$

$$\hat{S}(\hat{\Lambda}(\mathbf{x}))\left(i\hbar\hat{\gamma}^{\alpha}\Lambda^{\alpha'}{}_{\alpha}E_{\alpha'}{}^{\mu'}\tilde{\nabla}_{\mu'}\right)\hat{S}^{-1}(\hat{\Lambda}(\mathbf{x}))\psi'(\mathbf{x}') - mc\,\psi'(\mathbf{x}') = 0$$

$$\left[i\hbar\hat{S}(\hat{\Lambda}(\mathbf{x}))\hat{\gamma}^{\alpha}\Lambda^{\alpha'}{}_{\alpha}\hat{S}^{-1}(\hat{\Lambda}(\mathbf{x}))\tilde{\nabla}_{\mu'} - mc\right]\psi(\mathbf{x}) = 0\,, \tag{2.71}$$

The comparison of Eq. (2.71) with the original representation (2.68) has brought back the identical expression of flat spacetime, given by Eq. (2.22), except that $\hat{S}(\hat{\Lambda}(\mathbf{x}))$ here is local and that another transformation has been imposed on the *spinor connection field* $\hat{B}_{\mu}(\mathbf{x})$.

Simply put, the invariance under a local Lorentz transformation and and general coordinate transformation for the Dirac equation in curved spacetime is achieved by

$$\begin{aligned} \hat{\gamma}^{\alpha'} &= \hat{S}\hat{\gamma}^{\alpha}\Lambda^{\alpha'}{}_{\alpha}\hat{S}^{-1} \\ B_{\mu'} &= \hat{S}^{-1}B_{\mu}\hat{S} + \hat{S}^{-1}(\partial_{\mu}\hat{S})\,. \end{aligned} \tag{2.72}$$

As a final point, the connection field $B_{\mu}(\mathbf{x})$ has to be given an explicit expression, which can be derived by considering an infinitesimal Lorentz transformation

$$\Lambda^{\alpha}{}_{\beta} = \delta^{\alpha}{}_{\beta} + \epsilon^{\alpha}{}_{\beta}(\mathbf{x})\,, \tag{2.73}$$

where $\epsilon_{\alpha\beta}$ is antisymmetric, but in comparison to Eq. (2.23) depends on spacetime. The matrix $\hat{S}(\hat{\Lambda}(\mathbf{x}))$ in this form is given by

$$\hat{S}(1+\epsilon) = 1 + i\,\epsilon^{\alpha\beta}\Sigma_{\alpha\beta}\,. \tag{2.74}$$

The following derivation and argumentations has been found in [10]. Inserting the infinitesimal form (2.74) for $\hat{S}(\hat{\Lambda}(\mathbf{x}))$ into the transformation relation of $\hat{B}_{\mu'}$, gives to first order in $\epsilon^{\alpha\beta}$

$$B_{\mu'}(\mathbf{x}) = B_{\mu}(\mathbf{x}) + i\epsilon^{\alpha\beta}\left[\Sigma_{\alpha\beta}, B_{\mu}(\mathbf{x})\right] - i\partial_{\mu}\epsilon^{\alpha\beta}\Sigma_{\alpha\beta}\,. \tag{2.75}$$

"The connection should take its value in the Lie algebra of $SO(1,3)$", so B_{μ} may be written

$$\hat{B}_\mu(\mathbf{x}) = B_\mu{}^{\alpha\beta}(\mathbf{x})\Sigma_{\alpha\beta}\,. \tag{2.76}$$

Inserting this ansatz into the Eq. (2.75) gives

$$B_{\mu'}{}^{\alpha\beta} = B_\mu{}^{\alpha\beta} + B_\mu{}^\beta{}_\gamma\,\epsilon^{\gamma\alpha} - B_\mu{}^\alpha{}_\gamma\,\epsilon^{\gamma\beta} - i\partial_\mu\epsilon^{\alpha\beta}\,. \tag{2.77}$$

This result can be compared with the transform of the spin connection Eq. (2.65), where the insertion of the infinitesimal Lorentz transformation Eq. (2.73) yields

$$\omega_{\mu'}{}^{\alpha\beta} = \omega_\mu{}^{\alpha\beta} + \omega_\mu{}^\beta{}_\gamma\epsilon^{\gamma\alpha} - \omega_\mu{}^\alpha{}_\gamma\epsilon^{\gamma\beta} - \partial_\mu\epsilon^{\alpha\beta}\,. \tag{2.78}$$

This term is identical to the previous equation, except in the last term. Thus, comparison of the connection and the field results in

$$B_\mu{}^{\alpha\beta} = i\,\omega_\mu{}^{\alpha\beta}\,. \tag{2.79}$$

This relation justifies the name *spin connection* for $\omega_\mu^{\alpha\beta}$, since the coefficients are used to properly transform the Dirac field with respect to local transformations. Another diligent derivation of this relation shows the link of the spin connection to the vierbein field [11]

$$\omega_\mu{}^\alpha{}_\beta = -E^\nu{}_\beta\tilde{\nabla}_\mu E_\nu{}^\alpha\,. \tag{2.80}$$

Finally, the covariant derivative of the spinor field can be written as

$$\begin{aligned}\tilde{\nabla}_\mu\psi(\mathbf{x}) &= (\partial_\mu + \hat{B}_\mu)\psi(\mathbf{x})\\ &= (\partial_\mu + i\omega_{\mu\alpha\beta}\Sigma^{\alpha\beta})\psi(\mathbf{x})\\ &\overset{(2.25)}{=} \left(\partial_\mu + \frac{1}{8}\omega_{\mu\alpha\beta}[\hat{\gamma}^\alpha,\hat{\gamma}^\beta]\right)\psi(\mathbf{x})\end{aligned} \tag{2.81}$$

and consequently the final form of the Dirac equation in a non-inertial frames is

$$\left[i\hbar\hat{\gamma}^\mu\left(\partial_\mu + \frac{1}{8}\omega_{\mu\alpha\beta}[\hat{\gamma}^\alpha,\hat{\gamma}^\beta]\right) - mc\right]\psi(\mathbf{x}) = 0\,. \tag{2.82}$$

2.1.3 Deriving the Spin Rotation coupling

The derivation of the spin rotation coupling from the generally covariant Dirac equation, given by Eq. (2.82), will be performed shortly on the basis of Ryder's article [16]. The prediction of an interaction of intrinsic spin with the angular frequency was made with respect to a non-inertial, rotating frame. Therefore one considers a frame rotating about the z-axis, with

$$t' = t \quad x' = x\,cos(\Omega t) - y\,sin(\Omega t) \quad y' = -x\,sin(\Omega t) + y\,cos(\Omega t) \quad z' = z\,, \tag{2.83}$$

where Ω is the real-valued, angular frequency. From the definition

$$ds^2 = \eta_{\alpha\beta} dx^\alpha dx^\beta = g_{\mu\nu} dx^\mu dx^\nu\,, \tag{2.84}$$

the Minkowski line element $ds^2 = c^2 dt'^2 - dx'^2 - dy'^2 - dz'^2$ in these coordinates becomes

$$ds^2 \overset{(2.83)}{=} \left[1 - \left(\frac{\Omega}{c}\right)^2 (x^2 + y^2)\right] c^2 dt^2 + 2\frac{\Omega}{c}(ydx - xdy)cdt - dx^2 - dy^2 - dz^2\,. \tag{2.85}$$

Defining the *cobasis* (2.28) as

$$\theta^0 = cdt \quad \theta^1 = dx - \Omega y dt \quad \theta^2 = dy + \Omega x dt \quad \theta^3 = dz\,, \tag{2.86}$$

puts the line element into the orthonormal form

$$ds^2 = \left(\theta^0\right)^2 - \left(\theta^1\right)^2 - \left(\theta^2\right)^2 - \left(\theta^3\right)^2\,. \tag{2.87}$$

Utilizing the orthonormality relation $\hat{\boldsymbol{e}}_{(\mu)} \otimes \hat{\boldsymbol{\theta}}^{(\nu)} = \delta^\nu_\mu$ (2.30) a rotating orthonormal tetrad can be obtained

$$e_0 = \frac{1}{c}\partial_t + \frac{\Omega y}{c}\partial_x - \frac{\Omega x}{c}\partial_y \quad e_1 = \partial_x \quad e_2 = \partial_y \quad e_3 = \partial_z\,. \tag{2.88}$$

At this point it is helpful to recall two important relations, which have been established in the previous sections

$$[\hat{\boldsymbol{e}}_{(\alpha)}, \hat{\boldsymbol{e}}_{(\beta)}] = C^{\gamma}{}_{\alpha\beta}\hat{\boldsymbol{e}}_{(\gamma)} \tag{2.46}$$

$$\omega_{\alpha\beta\mu} = -\frac{1}{2}\left(C_{\alpha\beta\mu} + C_{\beta\mu\alpha} - C_{\mu\alpha\beta}\right) . \tag{2.62}$$

It is evident that the only commutators that do not vanish are

$$[e_0, e_1] = \frac{\Omega}{c}\, e_2 = C^2{}_{01}\, e_2 \qquad [e_0, e_2] = \frac{\Omega}{c}\, e_1 = C^1{}_{02}\, e_1 \, . \tag{2.89}$$

With $C_{\alpha\beta\gamma} = \eta_{\alpha\delta}C^{\delta}{}_{\beta\gamma}$ the spinor coefficients are given by

$$\omega_{120} = -\omega_{210} = \frac{\Omega}{c} \, . \tag{2.90}$$

Finally, the spin connection matrices for this tetrad are given by $\hat{B}_i = 0$ and

$$\hat{B}_0 \overset{(2.81)}{=} \frac{1}{8}[\hat{\gamma}^{\alpha}, \hat{\gamma}^{\beta}]\omega_{\alpha\beta 0} = \frac{1}{4}\frac{\Omega}{c}[\hat{\gamma}^1, \hat{\gamma}^2] = -\frac{i}{2c}\,\Omega\Sigma^3 \, , \tag{2.91}$$

where $\Sigma^i \equiv diag(\hat{\sigma}^i, \hat{\sigma}^i)$. Thus the Dirac equation is given by

$$\left[i\hbar\hat{\gamma}^{\mu}\partial_{\mu} + \frac{1}{c}\gamma^0\frac{\hbar\Omega}{2}\Sigma^3 - mc\right]\psi(\mathbf{x}) = 0 \, , \tag{2.92}$$

from which an explicit form of the Hamiltonian in the rotating frame can be deduced by transforming back according to Eq. (2.12)

$$H_D' = mc^2\hat{\beta} - i\hbar c\,\hat{\alpha}^i\partial_i - \frac{\hbar\Omega}{2}\Sigma^3 \, . \tag{2.93}$$

The last term in given by Eq. (2.93) is the interaction of spin with the angular velocity of a frame rotating around the z-axis. An important insight, mentioned by Ryder [16] and Hehl & Ni [17], is that the tetrad Eq. (2.88) is a rotating tetrad in reference to Fermi-Walker transport. The condition of Fermi-Walker transport is [18]

$$\frac{dv^m}{d\tau} = u^i\nabla_i v^m = \left(u^m a^n - u^n a^m\right) v_n \, , \tag{2.94}$$

where u^i is the velocity and a^j the acceleration of an observer along a curve. A frame

that is Fermi-Walker transported defines a spatial triad $\hat{\boldsymbol{e}}_i$ which is not rotating. "It ensures that the tetrad remains orthonormal and the time direction coincides with the direction of the four velocity". The factor $(u^m a^n - u^n a^m)\, v_n$ accounts for the inevitable 'rotation' and *Fermi-Walker transport* ensures that there is no additional rotation of the spacial basis vectors" [18].
However it can be calculated [16] that $\nabla_0 e_1 = -\frac{\Omega}{c} e_1 \neq 0$, thus the frame is a rotating system.

2.2 Nonrelativistic limit and Foldy-Wouthuysen transformations

In the previous section it has been described that the coupling of spin to angular velocity arises in the relativistic case. An important requirement of relativistic theories is the derivation of physical laws in the non-relativistic limit. For that purpose a procedure is sought to find the non-relativistic limit of the Dirac Hamiltonian, which generates diagonal correction terms to arbitrary orders. One suited method for this aim is the *Foldy-Wouthuysen transformation* (FWT), whose central idea is the separation of positive and negative-energy states [19] and which can be used to find a proper Hamiltonian in the non-relativistic limit. This method is briefly explained in the following section.
The Dirac Hamiltonian can be grouped into two types of operators, odd $\hat{\mathcal{O}}$ and even $\hat{\mathcal{E}}$ operators. Odd operators couple large and small components of the Dirac spinor (e.g. $\hat{\alpha}^i$, γ^5), whereas an even operator has no such matrix elements (e.g. $\mathbb{1}$, $\hat{\beta}$, $\hat{\sigma}_i$). Every operator can be decomposed into a sum of an odd and an even operator. In the case of the Hamiltonian in Eq. (2.93)

$$H_D = \hat{\beta} mc^2 + \hat{\mathcal{E}} + \hat{\mathcal{O}}\,, \tag{2.95}$$

with $\hat{\mathcal{E}} = -\frac{\hbar\Omega}{2}\Sigma^3 = -\boldsymbol{\Omega}\boldsymbol{S}$ and $\hat{\mathcal{O}} = -i\hbar c\,\hat{\alpha}^i\partial_i = c\boldsymbol{\alpha}\boldsymbol{p}$. The ambition of the FWT is to find a unitary transformation, that "successively removes odd terms from the Hamiltonian to any desired order in $(1/mc^2)$". The decoupling is performed by

$$\psi' = e^{i\mathcal{S}}\psi\,, \tag{2.96}$$

where $\mathcal{S}$ can be in general time-dependent. Inerting this ansatz into the Dirac Hamiltonian in the Schrödinger form Eq. (2.3) yields

$$i\hbar\left(\partial_t e^{-i\mathcal{S}}\right)\psi' + i\hbar e^{-i\mathcal{S}}\partial_t\psi' = H_D e^{-i\mathcal{S}}\psi'\,. \tag{2.97}$$

Rearranging the terms

$$i\hbar\partial_t\psi' = \left[e^{i\mathcal{S}}\left(H_D - i\hbar\partial_t\right)e^{-i\mathcal{S}}\right]\psi' \equiv H_D'\psi'\,, \tag{2.98}$$

delivers the form of the FWT

$$H_D' = e^{i\mathcal{S}}\left(H_D - i\hbar\partial_t\right)e^{-i\mathcal{S}}\,. \tag{2.99}$$

This formula can be expanded into a series of nested commutators by *Hadamard's Lemma* (see *Baker-Campbell-Hausdorff* formula)

$$\begin{aligned} e^X Y e^{-X} &= \sum_m^\infty \frac{1}{m!}[X,Y]_m \\ &= Y + [X,Y] + \frac{1}{2!}\left[X,[X,Y]\right] + \frac{1}{3!}\left[X,[X,[X,Y]]\right] + \cdots\,, \end{aligned} \tag{2.100}$$

where $[X,Y]_0 \equiv Y$ and $[X,Y]_m \equiv [X,[X,Y]_{m-1}]$. Applying this on the Hamiltonian given by Eq. (2.99) for the case that $\mathcal{S}$ is time-independent yields to second order

$$H_D' = H_D + [i\mathcal{S}, H_D] + \frac{1}{2}\left[i\mathcal{S},[i\mathcal{S},H_D]\right] + \,\cdots\,. \tag{2.101}$$

From this the non-relativistic approximation can be calculated with the canonical transformation for $\mathcal{S}$, given by

$$\mathcal{S} = -\frac{i}{2mc^2}\hat{\beta}\hat{\mathcal{O}}\,. \tag{2.102}$$

The first commutator of H_D' is

$$\begin{aligned} [i\mathcal{S}, H_D] &= i\left[\frac{-i}{2mc^2}\hat{\beta}\hat{\mathcal{O}}, \left(\hat{\beta}mc^2 + \hat{\mathcal{E}} + \hat{\mathcal{O}}\right)\right] \\ &= \frac{1}{2mc^2}\left([\hat{\beta}\hat{\mathcal{O}},\hat{\beta}]mc^2 + [\hat{\beta}\hat{\mathcal{O}},\hat{\mathcal{E}}] + [\hat{\beta}\hat{\mathcal{O}},\hat{\mathcal{O}}]\right)\,. \end{aligned} \tag{2.103}$$

The product of two even matrices or of two odd matrices is an even matrix, while the product of an odd matrix and an even matrix is an odd matrix. Furthermore $\hat{\beta}$ commutes with all even matrices $[\hat{\beta}, \hat{\mathcal{E}}] = 0$ and anti-commutes with all odd operators $\{\hat{\beta}, \hat{\mathcal{O}}\} = 0$. Thus, the three commutators in Eqs. (2.103) are given by

$$\begin{aligned}
[\hat{\beta}\hat{\mathcal{O}}, \hat{\beta}] &= -2\hat{\mathcal{O}} \\
[\hat{\beta}\hat{\mathcal{O}}, \hat{\mathcal{E}}] &= \hat{\beta}[\hat{\mathcal{O}}, \hat{\mathcal{E}}] \\
[\hat{\beta}\hat{\mathcal{O}}, \hat{\mathcal{O}}] &= 2\hat{\beta}\hat{\mathcal{O}}^2
\end{aligned} \tag{2.104}$$

and the commutator relation Eq. (2.103) becomes

$$[i\mathcal{S}, H_D] = -\hat{\mathcal{O}} + \frac{1}{2mc^2}\hat{\beta}[\hat{\mathcal{O}}, \hat{\mathcal{E}}] + \frac{1}{mc^2}\hat{\beta}\hat{\mathcal{O}}^2 \,. \tag{2.105}$$

The first term in this expression is $-\hat{\mathcal{O}}$, which inserted into the FW- Hamiltonian in Eq. (2.101) erases the odd operator to first order in H_D', so that odd matrices only occur in orders of $\frac{1}{mc^2}$ and smaller, thus

$$H_D' = \hat{\beta}mc^2 + \hat{\mathcal{E}} + \frac{1}{2mc^2}\hat{\beta}[\hat{\mathcal{O}}, \hat{\mathcal{E}}] + \frac{1}{mc^2}\hat{\beta}\hat{\mathcal{O}}^2 + \frac{1}{2}\left[i\mathcal{S}, [i\mathcal{S}, H_D]\right] + \cdots \,. \tag{2.106}$$

It is possible to evaluate the commutators of higher orders and separate the new operator again into odd and even components $H_D'' = \hat{\beta}mc^2 + \mathcal{E}' + \mathcal{O}'$. However, instead of exploring this further, the result of the Hamiltonian to order of $\frac{1}{mc^2}$ is given here following reference [19], where the derivative $\dot{\mathcal{S}}$ has been set zero ($\dot{\mathcal{S}} = 0$), so

$$H_D' = \hat{\beta}mc^2 + \mathcal{E} + \frac{1}{2mc^2}\left(\hat{\beta}\mathcal{O}^2 + \hat{\beta}[\mathcal{O}, \mathcal{E}]\right) + \cdots \,. \tag{2.107}$$

With $\mathcal{O}^2 = c^2(\boldsymbol{\alpha}\mathbf{p})^2 = c^2\mathbf{p}^2$ the Hamilton operator in the lowest order reduces to three terms, i.e the rest mass, the kinetic energy and the spin - rotation coupling

$$H = \hat{\beta}mc^2 + \hat{\beta}\frac{\mathbf{p}^2}{2m} - \boldsymbol{\Omega}\boldsymbol{S} \,. \tag{2.108}$$

Two asides shall be made here. First, this derivation has been performed in a very close analogy to the paper of Hehl & Ni [17]. Thereby they have used a frame that is subjected to both rotation $\boldsymbol{\Omega}$ and acceleration $\boldsymbol{a}$. In the non-relativistic approximation they found the solution to a more general case

$$\begin{aligned} H = \hat{\beta}mc^2 + \hat{\beta}\frac{\mathbf{p}^2}{2m} + \hat{\beta}m(\mathbf{a}\cdot\mathbf{r})\frac{\hat{\beta}}{2mc^2}\mathbf{p}\,(\mathbf{a}\cdot\mathbf{r})\cdot\mathbf{p} \\ -\boldsymbol{\Omega}\cdot(\mathbf{L}+\mathbf{S}) + \frac{\hbar}{2mc^2}\hat{\boldsymbol{\sigma}}(\mathbf{a}\times\mathbf{p}) + \text{higher-order terms}\,, \end{aligned} \tag{2.109}$$

witch for $\mathbf{L} = 0$ and $\mathbf{a} = 0$ reduces to the previous equation (2.108). Secondly, it has been alluded to the fact that the FWT's central idea is to separate the positive and negative energy states of the Dirac field. Consequently, it is actually possible to find a solution that is valid at all energies. The retrieval of an relativistic exact form of the Foldy-Wouthuysen in the special case of a Hamiltonian with spin-rotation coupling can be found in [20].

Eventually, there is a quantum-classical analogue to the spin-rotation coupling. The motion of a particle with magnetic moment $\boldsymbol{\mu}$ in the presence of an uniform external magnetic field $\mathbf{B}$ is given by the Hamiltonian

$$H_P = H_0 + \frac{q}{mc}\mathbf{p}\cdot\mathbf{A} - \boldsymbol{\mu}\cdot\mathbf{B}\,, \tag{2.110}$$

where $\mathbf{A} = \frac{1}{2}\mathbf{B}\times\mathbf{r}$ is the vector potential [21].

2.3 Interaction of free neutrons with magnetic fields

After the implementation of the mathematical foundations of the spin rotation coupling, the theory of the applicative part is described here. For the experiment described in chapter 4 the behaviour of neutrons in magnetic fields has to be analyzed.

To measure observational effects of the spin-rotation coupling, a rotating frame of reference has to be arranged in the experiment. Instead of mechanically rotating, the neutrons' spins can be manipulated in magnetic fields, in this case a uniformly rotating field $\mathbf{B}(\Omega)$. The non-relativistic equation of motion for these neutrons is given by the *Pauli* equation Eq. (2.110), which in the non canonical form of the momentum operator is given by

$$\left[\frac{\hbar^2}{2m_n}\Delta + \mu\hat{\boldsymbol{\sigma}}\mathbf{B}\right]\psi(r,t) = -i\hbar\frac{\partial}{\partial t}\psi(r,t)\,, \tag{2.111}$$

where $\psi(r,t)$ is a two dimensional spinor wave function, analogue to the four dimensional spinor (2.9). From the definition of the time evolution of an operator in quantum theory

$$\frac{d}{dt}\langle\hat{A}\rangle = \langle\frac{\partial\hat{A}}{\partial t}\rangle - \frac{i}{\hbar}\langle[\hat{A},H]\rangle\ , \tag{2.112}$$

the *Larmor precession* can be deduced, by examining the evolution of the Pauli matrices

$$\frac{d}{dt}\langle\hat{\boldsymbol{\sigma}}\rangle = -\frac{i}{\hbar}\langle[\hat{\boldsymbol{\sigma}},H]\rangle = -i\frac{\mu}{\hbar}\langle[\hat{\boldsymbol{\sigma}},\hat{\boldsymbol{\sigma}}\mathbf{B}]\rangle\ . \tag{2.113}$$

From $[\hat{\sigma}_i,\hat{\sigma}_j] = 2i\epsilon_{ijk}\hat{\sigma}_k$ follows

$$\frac{d}{dt}\langle\hat{\boldsymbol{\sigma}}\rangle = -\frac{2\mu}{\hbar}\langle\mathbf{B}\times\hat{\boldsymbol{\sigma}}\rangle \equiv -\gamma\langle\mathbf{B}\times\hat{\boldsymbol{\sigma}}\rangle\ , \tag{2.114}$$

where $\gamma = 1.833\cdot 10^8$ [rad/ (s T)] is the gyromagnetic ratio of the neutron. For a spatially homogeneous field Eq. (2.114) can be written as

$$\frac{d}{dt}\langle\hat{\boldsymbol{\sigma}}\rangle = -\gamma\mathbf{B}\times\langle\hat{\boldsymbol{\sigma}}\rangle\ . \tag{2.115}$$

The polarization vector of a particle is the expectation value of its spin

$$\mathbf{P} = \langle\hat{\boldsymbol{\sigma}}\rangle = \langle\psi|\,\hat{\boldsymbol{\sigma}}\,|\psi\rangle\ . \tag{2.116}$$

Thus the relation Eq. (2.115) can also be written as

$$\dot{\boldsymbol{P}} = \mathbf{P}\times\gamma\mathbf{B}\,. \tag{2.117}$$

Formally, this equation has the same appearance as a classical magnetic dipole in a homogeneous magnetic field. This means that the polarization vector $\mathbf{P}$ precesses counterclockwise about the external magnetic field's momentary axis $\mathbf{B}$ with the angular Larmor frequency $\hat{\boldsymbol{\omega}}_L(t) = \gamma\mathbf{B}(t)$.

The definition of the polarization vector Eq. (2.116) can be generalized to an ensemble of mixed spin states. The expectation values have to be weighted with a clssical probabibility distribution, which motivates the definition of the *density matrix*

$$\hat{\rho} = \sum_i |\psi_i\rangle \, p_i \, \langle\psi_i| \ , \tag{2.118}$$

where p_i is the probability in the quantum system $|\psi_i\rangle$. The expectation value of a neutron beam with mixed spin state is given by

$$\mathbf{P} = \langle\hat{\boldsymbol{\sigma}}\rangle = Tr\left(\hat{\rho}\hat{\boldsymbol{\sigma}}\right) \ . \tag{2.119}$$

An important measure for the intermixture of the spin states is given by the *degree of polarization*

$$P = \frac{N_\uparrow - N_\downarrow}{N_\uparrow + N_\downarrow} \, . \tag{2.120}$$

For an unpolarized beam, the number of *up-spins* $N_\uparrow$ equals the number of *down-spins* $N_\downarrow$, thus $P = 0$. Pure spin states on the other hand are given in the case $P = 1 \ = \ 100\%$. The *degree of polarization* of the initial beam of neutrons is almost 100% and the mixture of the spin states will be neglected.
It is possible to find an analytic solution of Eq. (2.111) for

$$\mathbf{B}(\Omega, t) = \begin{pmatrix} B_0 \, cos\Omega t \\ 0 \\ B_0 \, sin\Omega t \end{pmatrix} \qquad \mathbf{B}(\Omega, t) = 0 \, \text{for} \, t < 0, t > T \, . \tag{2.121}$$

The proper derivation to the solution can be found in the appendix A. The wave function is given by

$$\psi(y, t, \Omega) = \frac{1}{\sqrt{2\pi}} e^{i\left(ky - \frac{\hbar k^2}{2m} t\right)} \, e^{i\frac{\Omega t}{2}\hat{\sigma}_y} \, e^{-\frac{i}{2}\,\boldsymbol{\alpha}\cdot\boldsymbol{\sigma}} \, \chi(0) \, . \tag{2.122}$$

This result has the significant role of describing the evolution of the rotating-spins in magnetic coils, which is further analyzed in section 3.3.

3 Experimental Concepts in neutron polarimetry

The following chapter will give a brief theoretical and practical explanation of the devices that have been used for the experiment. The tools and technicalities are more or less standards in neutron polarimetry. The content of the following subsections come mostly from the diploma thesis [22].

3.1 Neutron source

3.1.1 Reactor

The most common neutron sources that can supply high neutron fluxes and convenient measurement durations are atom reactors. Our experiment has been executed at the TRIGA Mark-II research reactor in Vienna. The characteristics of the reactor are in [23] or [24].
The maximum continous thermal power of the reactor is 250 kW$_{th}$. The fuel elements consists of 8%wt uranium with an U^{235} enrichment of 20%, 91%wt zirconium and 1%wt hydrogen providing a thermal neutron flux of $10^{13} cm^{-2} s^{-1}$ in the central irradiation tube. The term "thermal neutron" refers to a subdivision of the free neutron's kinetic energy, respectively the neutron velocity, that is analogue to their thermodynamic temperature (see Tab. 3.1). The corresponding conversion is used

$$E\,[\mathrm{meV}] = 5.2267 \cdot 10^{-6} v^2 = 0.086173\,T. \tag{3.1}$$

The nuclear chain reaction is initiated by a Sb-Be neutron source and controlled via three boron carbide rods, witch serve as absorbers. The insertion of the rods into the reactor core causes the reactor to get sub-critical due to following two possible nuclear

Energy [eV]	Velocity [m/s]	Temperature [K]	Subdivision
$< 10^{-5}$	< 40	< 0.1	ultra cold neutr.
10^{-5} - $5 \cdot 10^{-3}$	$40 - 1000$	$0.1 - 60$	cold neutr.
$5 \cdot 10^{-3}$ - 0.5	$10^3 - 10^4$	$60 - 6000$	thermal neutr.
0.5 - 10^3	$10^4 - 4 \cdot 10^5$	$6 \cdot 10^3 - 10^7$	epithermal neutr.
10^3 - 10^5	$4 \cdot 10^5 - 4 \cdot 10^6$	$10^7 - 10^9$	intermediate neutr.
10^5 - $2 \cdot 10^7$	$4 \cdot 10^6 - 6 \cdot 10^7$	$10^9 - 3 \cdot 10^{11}$	fast neutr.
$> 2 \cdot 10^7$	$> 6 \cdot 10^7$	$> 3 \cdot 10^{11}$	relativistic neutr.

Table 3.1: The neutrons' names are corresponding to their thermodynamic energies. Velocity and Temperature have been calculated according Eq. (3.1).

reactions

$$^{10}_{5}\mathrm{B} + ^{1}_{0}\mathrm{n} \rightarrow ^{7}_{3}\mathrm{Li} + ^{4}_{2}\mathrm{He} + 2.8MeV \tag{3.2}$$

$$^{10}_{5}\mathrm{B} + ^{1}_{0}\mathrm{n} \rightarrow ^{7}_{3}\mathrm{Li}^{*} + ^{4}_{2}\mathrm{He} + 2.3MeV\,. \tag{3.3}$$

Both of the nuclear absorption reactions are so called (α,n) - reactions, since an α - particle is emitted. These two decay channels occur with a probability of 94% in the first case (Eq. (3.2)) and 6% in the second case (Eq. (3.3)) [25]. The withdrawal of the absorber rods enables the fission of the uranium anew and increases the reactors power. The main moderation of the neutrons takes place in the irradiation tube due to the zirconium-hydride. This chemical compound has the advantage of a small absorption cross-section for neutrons and the special property of a moderating efficiency, that is temperature-dependent, making the nuclear reaction inherently safe at high power. After the neutrons exit the irradiation tubes, they are moderated in the water by collision with the hydrogen atoms.
In theory the physical properties of moderators are described by the 'mean logarithmic reduction of neutron energy per collision' ξ , which only depends on the atomic mass A [26]

$$\xi = \ln\left(\frac{E_0}{E}\right) = 1 + \frac{(A-1)^2}{2A}\ln\left(\frac{A-1}{A+1}\right)\,, \tag{3.4}$$

where E_0 is the initial energy of the neutron and E is the energy of the neutron after a collision. The number N of necessary collisions of the neutron that is required to reduce the kinetic energy from E_0 to E can be deduced from 3.4 [27]

$$N = \frac{1}{\xi}\ln\left(\frac{E_0}{E}\right) . \tag{3.5}$$

In Tab. 3.2 are shown some results for a moderation of neutrons from 2 MeV to thermal neutron energy for hydrogen, deuterium and carbon.

	H	D	C
mass [u]	1	2	12
ξ	1	0.73	0.16
N	18.20	25.09	115.34

Table 3.2: Moderation quality of hydrogen, deuterium and carbon. Neutron's and the hydrogen's mass are almost equal, which makes hydrogen a good moderator.

Eventually, the neutrons exit the reactor vessel through one of the beam holes. Further details and technical aspects can be received at [23].

3.2 Preparation of neutrons

3.2.1 Monochromator

The neutrons that emerge from the reactor have a typical Maxwell-Boltzmann distribution and therefore posses different wavelengths. To filter one particular, yet continuous neutron beam (in contrast to pulsed signals) out of a polychromatic ray, a monochromator has to be used. The ordinary way to achieve this is to use certain crystals and make use of Bragg's law, i.e.

$$n\,\lambda = 2\,d_{hkl}\sin(\theta) . \tag{3.6}$$

The list of constants are: n integer, determining the order of the reflecion of the incident beam at the n-th atomic lattice plane; λ is the wavelength; d_{hkl} spacing between the planes in the atomic lattice with h,k,l indicating the Miller indices and θ, angle of incidence.

In many cases the monochromators are made from mosaic crystals, i.e. blocks of small crystals aligned in the same orientation. The monochromator installed at the polarimeter beamline of the TRIGA Mark-II research reactor in Vienna is pyrolytic graphite, where the neutron beam has a 1st order wavelength of $\lambda_{(\mathrm{n}=1)} = 1.99$Å and a monochromaticity of $(\Delta\lambda)/(\lambda_{(\mathrm{n}=1)}) \cong 0.02$, which have been verified by time of flight measurements. To remove Bragg peaks of higher order the incident angle between the supermirrors and the neutrons' direction of flight has to be adjusted (see chapter 3.2.2). [28]

3.2.2 Suppermirror polarizer

An important issue for neutral particles for optical experiments is controlling and guiding them without loss, since they cannot be deflected with electric fields. Thermal and cold neutrons undergo optical effects, which includes the phenomenon of *total reflection* in so called *guide tubes*. They usually have the form of a rectangular cuboid and are made of highly polished glass, evaporated with layers of nickel, titanium, a nickel/titanium composite or another reflecting substance with a large nuclear scattering length b.
A major limitation is given by the critical grazing angle ϕ_c of the incident beam, which for single layer mirrors is very small. For Ni and a neutron wave length of $\lambda = 2$ Å the critical angle is $\phi_c \approx 0.2°$. To extend the range of reflection the mirrors are evaporated with a multilayer of reflecting material with varying refractive index and depth, where the diffraction maxima are given again by *Bragg's law*. Starting from the surface the lattice constant of the crystals successively increases to achieve constructive interference of the reflected waves. The concept of the multilayer is illustrated in Fig. 3.1.
If the supermirror's material is magnetic one can utilize this for the scattering process and also polarize the neutrons, i.e. prepare all particles to have the same spin states. Some elemental properties of nuclear and magnetic interaction are explained here.
The effective interaction responsible for the magnetic scattering is the magnetic potential $V_m = -\mu\hat{\boldsymbol{\sigma}}\mathbf{B}$. The corresponding magnetic scattering length p is related to the potential V_m by the following Fourier transform [29] (also [30])

$$p(\mathbf{Q}) = \frac{m_\mathrm{n}}{2\pi\hbar^2}\int e^{i\mathbf{Qr}} V_\mathrm{m}(\mathbf{r})\, d\mathbf{r}\,, \tag{3.7}$$

where $\mathbf{Q}$ is the momentum transfer. The second contribution to be considered is the scattering of bound nucleons with the neutrons. The interaction of a free neutron with a

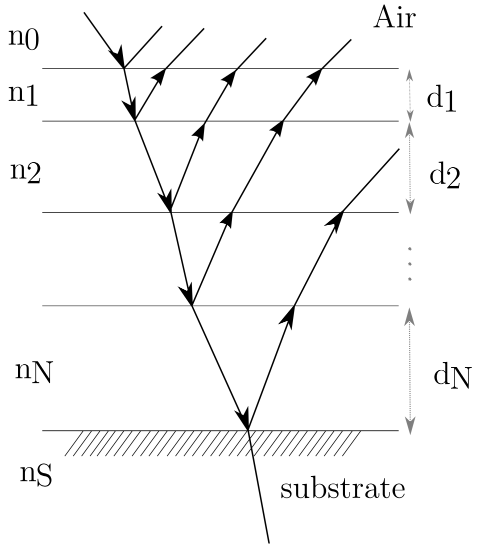

Figure 3.1: Schematic principle of a multilayer.

single, point-like nucleon was first introduced by Fermi [29] and is therefore called *Fermi pseudopotential* V_{n}

$$V_{\mathrm{n}}(\mathbf{r}) = \frac{m_{\mathrm{n}}}{2\pi\hbar^2} b\delta(\mathbf{r}) \,, \tag{3.8}$$

with b being the nuclear scattering length. This potential is presupposing isotropic wave scattering in the Born approximation and depends only on the nuclear scattering length b.

The magnitude of nuclear and magnetic scattering is determined by their respective scattering lengths. The reflectivity of the spin states {+,-} on a multi-bilayer with material A and B in the guide tube is given by

$$R_{\pm} \propto [N_A b_A - N_B(b_B \pm p_B)] \,, \tag{3.9}$$

For a suitable choice of materials ($b_B = \mp p_B$) the reflectivity of one spin component can be removed from the beam. A prominent couple of materials is Ni-Ti, which are also used in the *guide tubes* of this experiment. The Fig. 3.2 shows one of the supermirrors that has been used for the experiment.

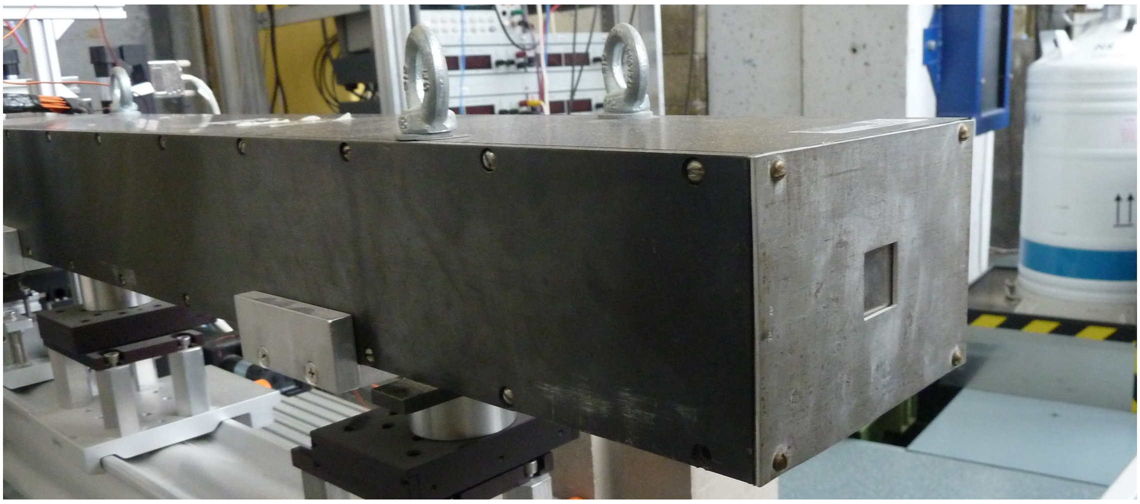

Figure 3.2: Real picture of the supermirrors, that were in use.

Since the critical angle

$$\phi_c = \lambda\sqrt{\frac{Nb}{2\pi}} \tag{3.10}$$

is proportional to the wavelength of the particles, a removal of higher wavelengths can be achieved by slightly changing the incident angle of the supermirror from the ideal value.

3.3 Neutrons in magnetic fields

After the neutrons have been prepared, they are led to the actual set-up. To understand how spin-dependent effects can be measured, the possibilities to control and manipulate the neutron spin in magnetic fields has to be investigated. A polarimeter consists of polarizer and analyzer together with spin-manipulator devices in between. Two kinds of coils are conventionally used; the *Helmholtz* coil for guiding the neutrons and stabilize them against exterior magnetic fields and the *spin rotator* coil to change the polarization.

3.3.1 The Helmholtz coil

The experiments with neutrons in a laboratory are usually exposed to the influences of external magnetic fields, for instance earth's magnetic field. To prevent the neutrons from depolarizing by this undesired fields, a magnetic shielding or a stronger, more

dominant guide field has to ensure the preservation of the initial polarization of the spin. Magnetic shielding with *mu-metal* has the disadvantage that the field lines are inhomogeneous at the frame of the shielding body. Therefore the method of the guiding field is favoured over the magnetic shielding.
The Helmholtz coils consist of a pair of two identical magnetic coils installed over the set-up. Ideally, the coils are separated by a distance that equals the radius of the coils in a circular arrangement. The Fig. (3.3) shows a small Helmholtz coil in a more rectangular form.

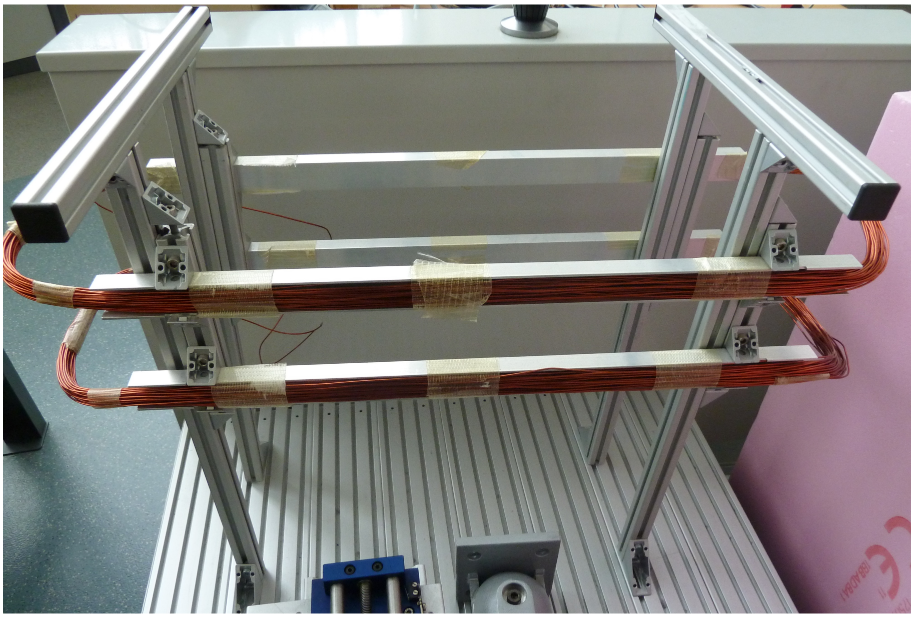

Figure 3.3: Smaller version of the Helmholtz coil, that was used during the experiment.

Since homogeneity of the field along the coil's axis is not given entirely in practice, it is favourable that the neutrons fly closely collimated along the middle in a small region, where the field in axial direction is almost constant. Furthermore the ends of the supermirrors are inserted in the guide field's region to prevent boundary effects of perturbing the constancy of the magnetic field.

3.3.2 Spin Rotator

The spin rotator is the most relevant tool of a polarimeter set-up. Essentially, it is a coil that provides a local magnetic field, where neutron spin and field interact. These spin rotators must have a suitable size to fit between the Helmholtz coils and are usually installed on tiltable plates to adjust their alignment relative to the direction of flight of the particle beam. The Fig. 3.4 shows two such coils that have been used in the experiment.

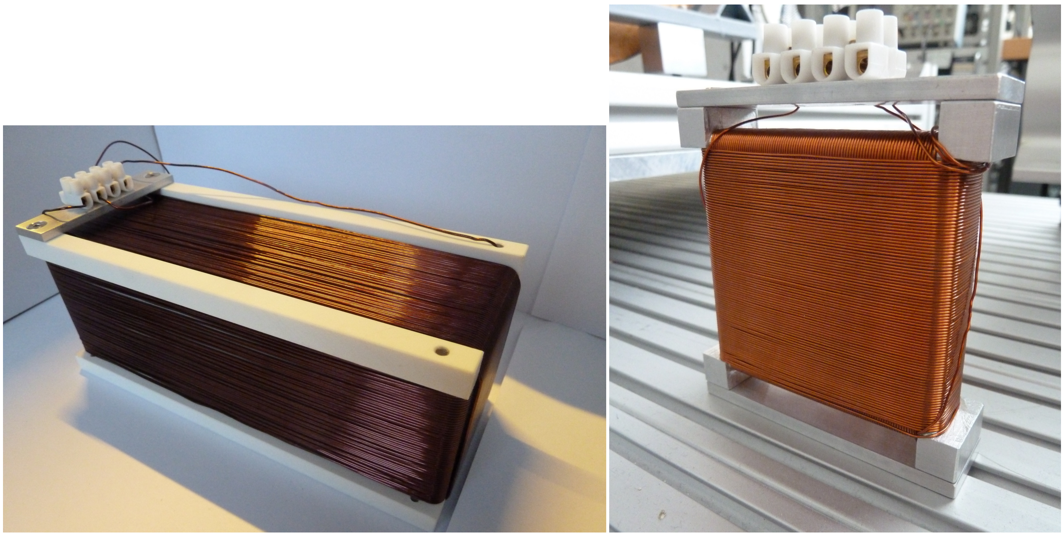

Figure 3.4: Two coils with 6 cm × 6 cm × 20 cm on the right side and 6 cm × 6 cm × 2 cm the left one.

Two cases of transitions can be distinguished for the neutrons that enter the coils, the adiabatic and the non-adiabatic case.

- Adiabatic case: The direction of the magnetic field changes spatially by a small amount, so that the polarization vector can follow the field configuration. The potential of the neutron is practically constant. This condition requires that the variation of the field, more precisely that the frequency of the change of this field ω_{var} is smaller than the *Larmor frequency* ω_L.

- Non-adiabatic case: The change of the magnetic field in the coil happens instantaneously for the neutrons. The polarization vector precesses about the new direction of the field, in which some spins are flipped, causing an energy splitting due to the *Zeeman effect*. This case is given for $\omega_{var} \gg \omega_L$.

Non-adiabatic transitions are used in our experiment to rotate the spins in the coil. For this purpose a magnetic field orthogonal to the direction of flight and the guide field is applied. If the influence of the guide field needs to be cancelled, a compensation field has to be implemented. The field configuration of a spin flipper is illustrated in Fig. 3.5.

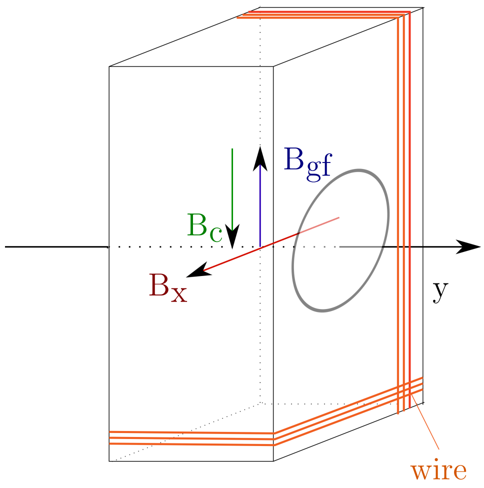

Figure 3.5: The neutrons fly in y-direction. On the x-Axis the B_x field is applied, inducing the spin rotation. The guide field B_{gf} by the Helmholtz coil, that is penetrating the coil, is locally compensated with B_c.

Since magnetic field lines form closed loops, the influence of the stray-field by B_x in the vicinity of the coil can make the polarization vector slightly tilt. This problem greatly depends on the form and the magnitudes of the fields in the coil. In section 4.3, this effect is described for our experiment.
The evolution of a neutron in a spin rotator flying in y-direction in an uniformly rotating field given by Eq. (2.121) has been given in the form Eq. (2.122), which in matrix form is given by

$$\psi(y,t,\Omega) = \frac{1}{\sqrt{2\pi}} e^{i\left(ky - \frac{\hbar k^2}{2m}t\right)} \begin{pmatrix} \cos\left[\frac{\Omega t}{2}\right] & \sin\left[\frac{\Omega t}{2}\right] \\ -\sin\left[\frac{\Omega t}{2}\right] & \cos\left[\frac{\Omega t}{2}\right] \end{pmatrix} \times$$

$$\times \begin{pmatrix} \cos\left[\frac{\alpha_1}{2}\right] & -\frac{(iB_0\gamma+\Omega)\sin\left[\frac{\alpha_1}{2}\right]}{B_{eff}\gamma} \\ \frac{(-iB_0\gamma+\Omega)\sin\left[\frac{\alpha_1}{2}\right]}{B_{eff}\gamma} & \cos\left[\frac{\alpha_1}{2}\right] \end{pmatrix} \chi(0)\,, \tag{3.11}$$

where the rotation angle $\alpha_1 = \alpha_1(t,\Omega,B_0)$ and the effective magnetic field B_{eff} are related by

$$\alpha_1(t,\Omega,B_0) = \pm\gamma t\sqrt{{B_0}^2 + \left(\frac{\Omega}{\gamma}\right)^2} \equiv \pm\gamma t B_{eff} \tag{3.12}$$

and $\chi(0)$ is the initial spin state. An analysis of Eq. (3.11) for an incident neutron with $\chi(0) = |+z\rangle$ suggests:

- $\Omega = 0$. Special case: *DC spin rotator*. The rotation of the field is turned off and only a static magnetic field in the x - direction is applied. As to be expected the wave function is

$$\psi(y,t) = \frac{1}{\sqrt{2\pi}} e^{i\left(ky - \frac{\hbar k^2}{2m} t\right)}\, e^{-i\frac{\alpha_1}{2}\sigma_x} \chi(0) \tag{3.13}$$

  and the polarization vector is rotating in the yz plane

$$\mathbf{P}(\alpha_1) = \begin{pmatrix} 0 \\ -\mathrm{Sin}[\alpha_1] \\ \mathrm{Cos}[\alpha_1] \end{pmatrix}. \tag{3.14}$$

- $\alpha_1 = 0$. For $\alpha_1 = 0 \rightarrow \Omega = B_0 = 0$. This is the trivial case with zero field, thus the coil is deactivated, the neutron preserves its original state

$$\psi(y,t) = \frac{1}{\sqrt{2\pi}} e^{i\left(ky - \frac{\hbar k^2}{2m} t\right)}\, \chi(0) \tag{3.15}$$

$$\mathbf{P}(\alpha_1 = 0) = \begin{pmatrix} 0 \\ 0 \\ 1 \end{pmatrix}. \tag{3.16}$$

- $\alpha_1 \neq 0$. *The AC spin rotator*. For a random rotation angle α_1 the polarisation vector with the following conditional dependence: $\Omega = 2\pi\nu = \sqrt{\left(\frac{\alpha_1}{t}\right)^2 - {B_0}^2\gamma^2}$ has components in all directions

$$\mathbf{P}(\alpha_1) = \begin{pmatrix} -\cos[\alpha_1]\sin[\Omega t] + \frac{\Omega\cos[\Omega t]\sin[\alpha_1]}{\gamma B_{\mathrm{eff}}} \\ -\frac{\sin[\alpha_1] B_0}{B_{\mathrm{eff}}} \\ \cos[\alpha_1]\cos[\Omega t] + \frac{\Omega\sin[\alpha_1]\sin[\Omega t]}{\gamma B_{\mathrm{eff}}} \end{pmatrix}. \tag{3.17}$$

- $\alpha_1 = n\,\pi$. Special case, where α_1 is a multible of π and the polarization has no value in the y-component.

$$\mathbf{P}(\alpha_1 = n\,\pi) = (-1)^n \begin{pmatrix} -sin[\Omega t] \\ 0 \\ cos[\Omega t] \end{pmatrix} . \qquad (3.18)$$

In case that n is odd, the coil acts as a *spin flipper*.

3.4 Detector

At the end of the set-up the neutrons enter the detector and are detected. Since neutrons have no charge a conversion process is needed, in which the emission of ionized particles is triggered. A gas proportional detector, filled with elements that have a high cross-section for thermal neutrons, e.g. BF_3 or ^3He, are conventional detectors for neutrons. Our detector is a BF_3 detector. The nuclear reaction for boron has been given in Eqs. (3.2), (3.3). This compound is suited for the detection of slow neutrons, because of its proportional behaviour, high natural abundance of boron and higher signal heights, leading to lower noise. Naturally, these tube-shaped detector are surrounded by moderating materials, which drastically increases the volume of the detector. The Fig. (3.6) shows the BF_3 detector of our experiment.

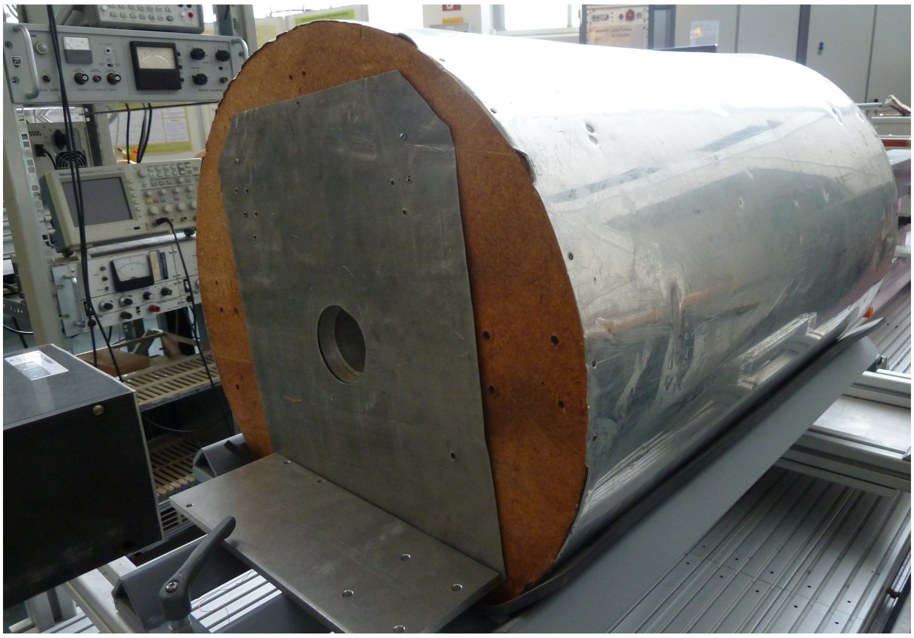

Figure 3.6: The actual BF_3 detector is very small. The shielding contributes the most to the volume of the detector. Cables at the back side lead to computers for data processing.

3.5 Some examples of neutron-polarimeter experiments

Neutron polarimetry plays an outstanding role in the determination of quantum-mechanical effects. Brief descriptions of examples shall illustrate how this method has helped to discover and measure interesting phenomenons.

A measurement of geometric phase in a neutron polarimeter

A quantum particle acquires generally a total phase consisting of a dynamical phase and a geometrical phase (also known as *Berry's phase*). This geometric phase only depends on the evolution path of quantum states, not on dynamical properties like time or energy [31]. An investigation of the geometric and dynamical phase of neutrons in a polarimetry has been reported [32]. The arrangement of the set-up is illustrated in Fig. 3.7.
In this experiment, conducted at the TRIGA Mark-II reactor of the Atominstitut, lots of efforts are made to discern the geometric phase from the much larger dynamical phase. The polarized neutrons generate exactly half a Larmor precession in R_1 and are converted from $|+z\rangle$ into $|+y\rangle$, so that the spin state becomes a superposition of $|+z\rangle$ and $|-z\rangle$. In the first arrangement the spin flippers are rotated about the same angle,

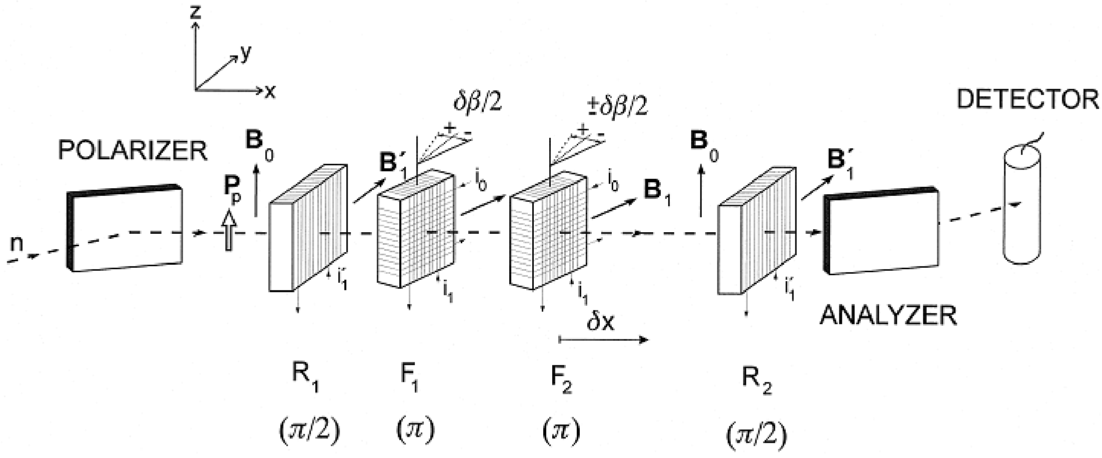

Figure 3.7: Schematic sketch of the polarimeter experiment as depicted in [32]. The spins are prepared in $|+z\rangle$ - states in the supermirror polarizer and a guide field is applied over the set-up. Four coils are used. R_1 converts the spin from $|+z\rangle$ into $|+y\rangle$ state and R_2 $|+y\rangle$ back into $|+z\rangle$. The F_1 and F_2 spin flippers, are not parallel, but slightly detuned by an angle $\delta\beta$. An translation δx of F_2 is performed before the neutrons are analyzed in the second supermirror and detected.

thus no geometric phase is induced. In a second set the spin flippers are rotated each by and angle $\delta\beta/2$ in opposite direction along the z-axis. The occurrence of a geometrical phase shift can be visualized on a so called *Bloch sphere* (also called *Poincaré sphere*), which is illustrated in Fig. 3.8. The incident $|+z\rangle$ state traverses a π flip at an angle β_1, which corresponds to a geodesic semi - great circle from the 'north pole' to the 'south pole'. After the flip in F_1 the spin $|+z\rangle$ and $|-z\rangle$ precesses about the guide field by $\phi_\uparrow$ and $\phi_\downarrow$ respectively, before the spin states traverse back due to the second π flip in F_2 oriented at the angle β_2. This cyclic evolution on the sphere is corresponding to the geometrical phase Φ_G, which is half the solid angle Ω_{12}

$$\Phi_G = -\frac{\Omega_{12}}{2} = \delta\beta\,, \tag{3.19}$$

whereas the dynamical phase is equal to $(\phi_\uparrow - \phi_\downarrow)/2$.

In their final results a linear dependence of the dynamical phase due to the translation of the coil F_2 and the geometric phase variation due to rotations of the coils F_1 and F_2 are

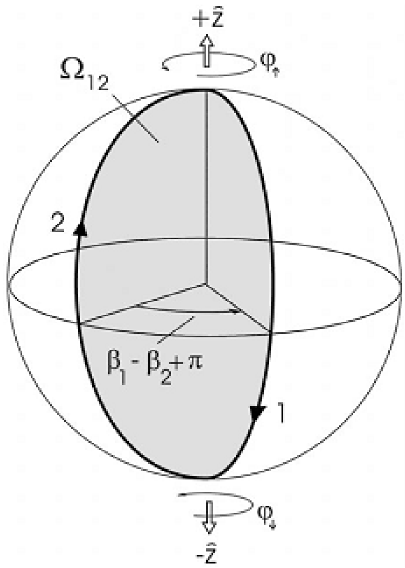

Figure 3.8: Illustration of the geometric phase on the *Bloch sphere* as found in [32]. The solid angle Ω_{12} is given by the paths **1** and **2**, which span a plane from $|+z\rangle$ to $|-z\rangle$ on the sphere. The horizontal fields in the spin flippers are oriented at angles β_1 and β_2. The guide field between F_1 and F_2 make the spin $|+z\rangle$ and $|-z\rangle$ precesses about the guide field by $\phi_\uparrow$ and $\phi_\downarrow$ respectively.

observed. The results of the dynamical phase and geometric phase shifts are illustrated in Fig. 3.9. Least square fits of the data exhibit the high level of accuracy, which show an improved by 23% in comparison to previous interferometer measurements (see [33] in [32]). The phase shifts agree with theory within about 1%.

Demonstration of the noncommutation properties of the Pauli spin operator in a neutron polarimeter.

Another example of a neutron polarimetric measurement has been published in [34], where the non-commutation of the Pauli matrices are demonstrated. A schematic illustration of the experiment is shown in Fig. 3.10.

The incident neutrons are polarized and the set-up is arranged in a guide field to minimize depolarization. The spin-turn devices enable to give the polarization vector an arbitrary orientation. Two spin rotators work in the middle of the experiment and can be rotated in the xz-plane to realize a rotation $U_R(\hat{\boldsymbol{\alpha}}_A)$ in the $\hat{\boldsymbol{\alpha}}_A$ direction and $U_R(\hat{\boldsymbol{\alpha}}_B)$ in the $\hat{\boldsymbol{\alpha}}_B$ direction respectively. The rotation has still to maintain a π flip. An orientation of the

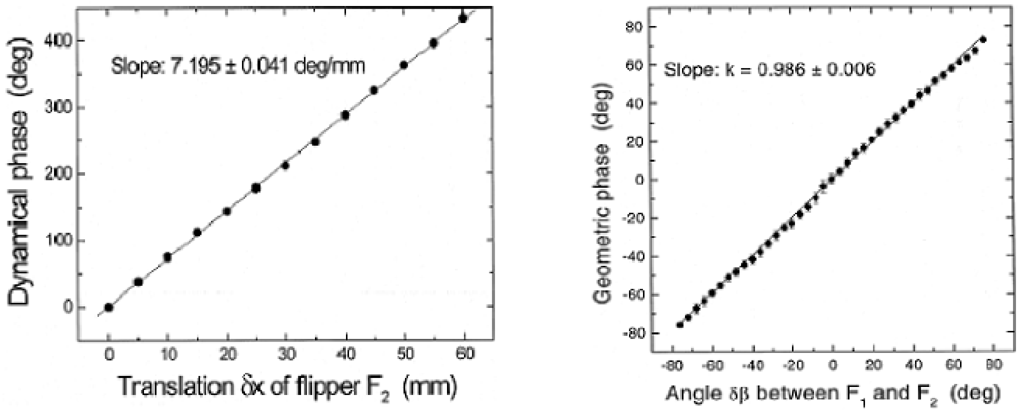

Figure 3.9: Plots of the obtained dynamical and geometrical phases [32]. The left plot shows the pure geometric phase Φ_D as a function of the translation δx of the flipper F_2. On the right, the observed geometric phase as a function of the angle $\delta\beta$ between the flippers.

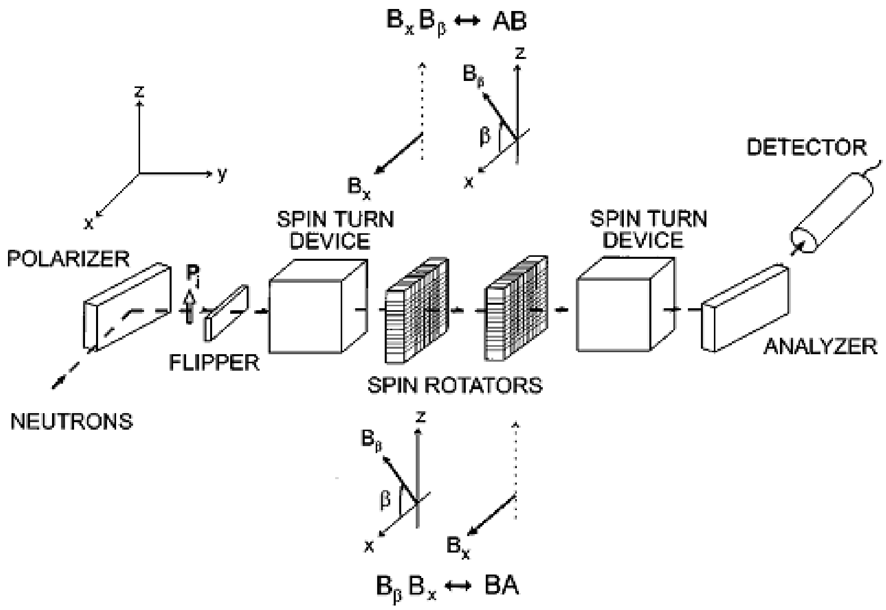

Figure 3.10: Experimental arrangement as depicted in [34]. The spin turn devices enable to give the polarization vector an arbitrary orientation. The spin rotators turn the spin in the sequential orders AB and BA in the directions $\hat{\boldsymbol{\alpha}}_A$ and $\hat{\boldsymbol{\alpha}}_B$.

magnetic field in +x direction corresponds to $\hat{\boldsymbol{\alpha}}_A = (1, 0, 0)$ and for a field in the xz plane to $\hat{\boldsymbol{\alpha}}_B = (cos(\beta), 0, sin(\beta))$, which give the following π flip operators

$$
\begin{aligned}
A &\equiv U_R(\hat{\boldsymbol{\alpha}}_A) = -i\hat{\boldsymbol{\sigma}}_x \\
B &\equiv U_R(\hat{\boldsymbol{\alpha}}_B) = -i\left(\hat{\boldsymbol{\sigma}}_x cos(\beta) + \hat{\boldsymbol{\sigma}}_z sin(\beta)\right) .
\end{aligned}
\tag{3.20}
$$

The normalized spin state $|\chi\rangle$ of the neutron can be described by

$$
|\chi\rangle = \begin{pmatrix} \cos[\theta/2] \\ e^{i\phi}\sin[\theta/2] \end{pmatrix} , \tag{3.21}
$$

where θ and ϕ are the polar and azimuthal angle. The final polarization vectors after the passage of the coil for the wave-functions $|\chi_{BA}\rangle = BA\,|\chi\rangle$ and $|\chi_{AB}\rangle = AB\,|\chi\rangle$ are given by

$$
\mathbf{P}_{BA} = \langle\chi_{BA}|\,\hat{\boldsymbol{\sigma}}\,|\chi_{BA}\rangle = \begin{pmatrix} \sin[\theta]\cos[\theta]\cos[2\beta] - \cos[\theta]\sin[2\beta] \\ \sin[\theta]\sin[\phi] \\ -\sin[\theta]\cos[\theta]\cos[2\beta] + \cos[\phi]\cos[2\beta] \end{pmatrix} \tag{3.22}
$$

and

$$
\mathbf{P}_{AB} = \langle\chi_{AB}|\,\hat{\boldsymbol{\sigma}}\,|\chi_{AB}\rangle = \begin{pmatrix} \sin[\theta]\cos[\theta]\cos[2\beta] + \cos[\theta]\sin[2\beta] \\ \sin[\theta]\sin[\phi] \\ \sin[\theta]\cos[\theta]\cos[2\beta] + \cos[\theta]\cos[2\beta] \end{pmatrix} . \tag{3.23}
$$

A mutual interchange of the two magnetic regions will therefore result in different final polarization state due to the non-commuting Pauli matrices.

The experiments show the results for incident neutrons polarized either in +z or -z direction, whose final polarization vectors are given by $\mathbf{P}_{AB} = (\pm\sin(2\beta), 0, \pm\cos(2\beta))$ and $\mathbf{P}_{BA} = (\mp\sin(2\beta), 0, \pm\cos(2\beta))$. The final results show that, as theory predicts, commutation of the two spin rotation operators leads to an inverse modulation of the x component for both initially $|+z\rangle$ and $|-z\rangle$ states. The plots in Fig. 3.11 show the different phase shifts induced by the actions of the operators AB and BA as a function of the angle β. Writing the evolution of the spin states as a superposition of the $|\pm y\rangle$ states shows that different phase shifts $\pm\beta$ are accumulated in $|\pm y\rangle$. "The final states depends on the intermediate states, that is, on the chosen trajectory in spin space" [34].

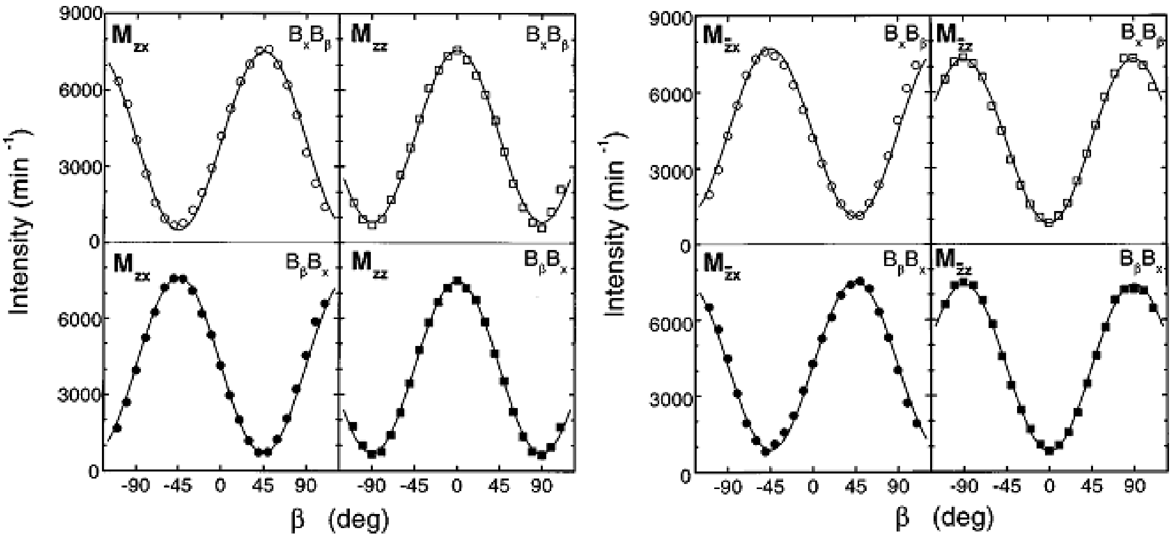

Figure 3.11: Results as illustrated in [34]. There are no dependence on the angle β of the z-polarization components, but the modulations of the x-components yields an inverse modulation.

The set-up of our experiment will be in close analogy to the examples given above and contain equivalent considerations. One of the major differences will be the application of a rotating magnetic field, instead of DC-coils only. The next chapter will deal with the measurement of the spin-rotation effect in a neutron polarimeter.

4 Measurement of the spin-rotation coupling

4.1 Original proposal and adoption to a polarimeter

An observable measurement of the spin-rotation coupling has first been proposed in [1] and later in [35] for a neutron interferometer experiment. An explanation of the original concept makes it easier to grasp the idea of the polarimeter set-up.

The original set-up: Polarized neutrons are split into two arms of a *Mach- Zehnder* type interferometer. Each of the two paths contain a spin flipper. Along one arm is a static spin flipper, while the other arm has a spin flipper which is slowly rotating parallel to the neutron wave vector. Instead of mechanically rotating, the idea of using a quadrature coil, which produces a rotating magnetic field $\mathbf{B}(\Omega)$, has been suggested at a later date in the paper [6].
Both spin flippers are aligned parallel and adjusted to induce a flip of the neutrons' spin, thus initially up spins become down spins after the flipper. Subsequently, the neutron beams recombine again and are measured in the detectors. If the 180° flipped neutrons in the static and in the rotating coil behave the same, then no change of the interferometer fringes are expected. However, if the rotating coil creates a phase shift due to spin-rotation coupling, the interference fringes will shift. The top sketch in Fig. 4.1 depicts the fundamental idea.

Intermediate set-up: In the first set-up the interferometer arm with the static coils serves as a reference for the rotating coil. Instead of a static coil, another spin flipper rotating in opposite direction could be installed. This would induce positive and negative phase shifts in each arm of the interferometer, thus doubling the contribution from the spin-rotation effect. See the middle of Fig. 4.1.

The same phase shift would arise if the initial neutrons were anti-parallel and would rotate in the same direction. This perspective can be easily transferred to the concept of a polarimeter.

Polarimeter set-up: One of the interferometer arms is removed, instead of a two-path superposition a two-spin superposition is utilized, which is illustrated at the bottom of figure 4.1. The second path of the interferometer is no longer the reference system, but rather the spin compared to the other one. The phase shift no longer modulates the intensity of an interference pattern, but reveals itself as a change of the polarization vector of the neutron.

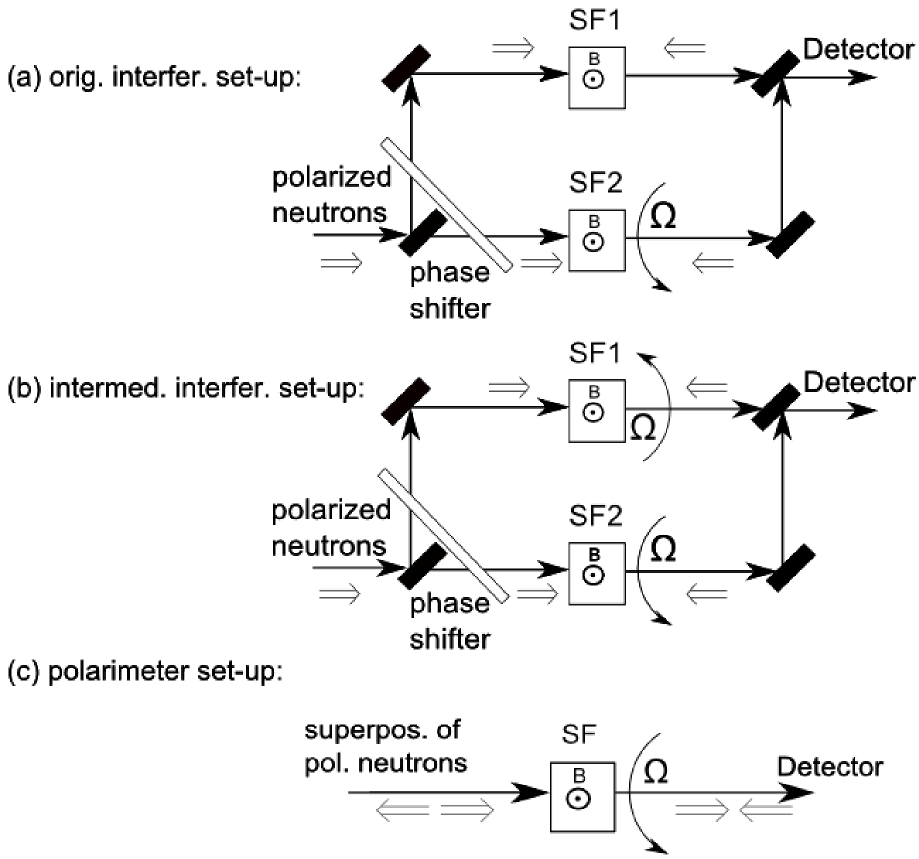

Figure 4.1: Simple black arrows imply flight directions and void arrows the spin state. SF1 and SF2 are the respective spin flippers, of which one is rotating. Original set-up at the top (a). The intermediate set-up in the middle (b) serves as an aid to understand the concept of the polarimeter experiment (c), depicted at the bottom.

In comparison with a polarimeter strategy set-up, an interferometer set-up has more limitations. The largest size of a neutron interferometer is roughly 30 cm, making it hard to place two bigger coils between the silicon crystals. Also the interferometer is extremely sensitive over mechanical movements and temperature fluctuations. To get a decent contrast a high flux has to be provided to compensate for the inevitably high loss of neutrons in interferometer experiments. All of these issues can be overcome by employing a polarimeter experiment.

4.2 A priori results

The following calculations enable to predict the evolution of the spin in the polarimeter and optimize the parameters for the actual measurement. As convention the wave vector of the neutron is chosen in the $+\hat{\mathbf{y}}$-direction and the guide field in the $+\hat{\mathbf{z}}$-direction. The central element of the experiment is the quadrature coil with the rotating field. The spin-rotation interaction will be described via the magnetic potential according to the *Pauli* equation (2.111), thus $\mathbf{S} \cdot \boldsymbol{\Omega} \rightarrow \hat{\boldsymbol{\sigma}} \cdot \mathbf{B}(\Omega)$. The solution to this problem is given by Eq. (2.122) or equivalently Eq. (3.11). The 3D graphic of the arrangement in Fig. 4.2 makes the comprehension of the following calculations easier.

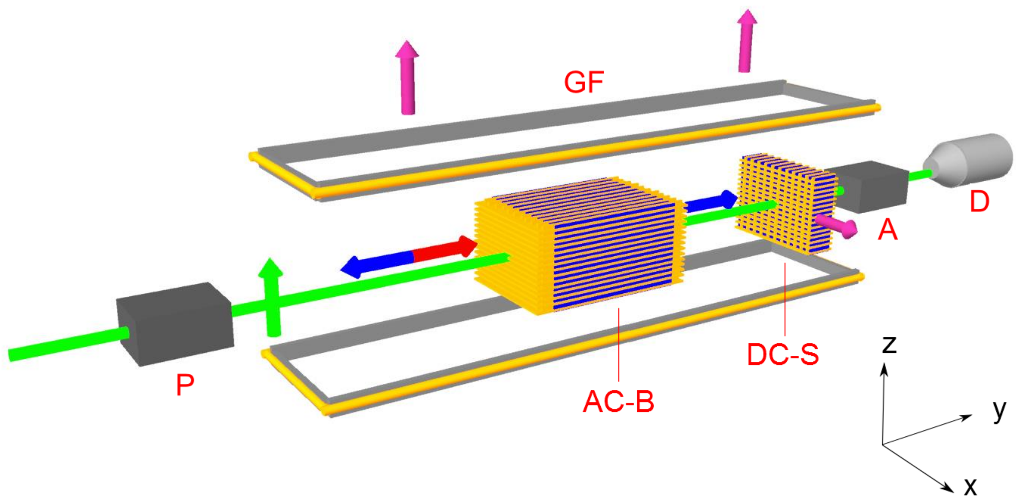

Figure 4.2: 3D model of the initial set-up. (P) 1st supermirror polarizer; (GF) guide field; (AC-B) Big AC-coil; (DC-S) Scanning DC-coil; (A) 2nd supermirror analyzer; (D) detector.

The superposition of the incident neutron can be represented as a $\chi(0) = |+z\rangle = \frac{1}{\sqrt{2}}(|+y\rangle + |-y\rangle)$. In the previous exemplification the rotation angle α_1 of the spin has been set to 180°, but further calculation will consider a 2π rotation instead, so the evolution of the spin parallel $|+y\rangle$ and anti-parallel $|-y\rangle$ to the flight direction after a $\alpha_1 = 2\pi$ yields

$$
\begin{aligned}
|+y\rangle(t_1) &= -e^{-i\frac{\hbar k^2}{2m}t_1}\, e^{\frac{i\Omega t_1}{2}}\, |+y\rangle \\
|-y\rangle(t_1) &= -e^{-i\frac{\hbar k^2}{2m}t_1}\, e^{\frac{-i\Omega t_1}{2}}\, |-y\rangle\ .
\end{aligned}
\tag{4.1}
$$

A 2π rotation of the spin obviously results in an additional frequency-dependence, where the parallel and anti-parallel states have the same phase shift with opposite signs. The minuses of the functions come from the 4π periodicity of the spinor.
Putting the wave-function together yields

$$
\begin{aligned}
\psi(y, t_1, \Omega) = \phi(y)\,\chi_1(t_1, \Omega) &= \frac{-1}{\sqrt{2\pi}} e^{i\left(ky - \frac{\hbar k^2}{2m}t_1\right)}\, \frac{1}{\sqrt{2}} \left(e^{i\frac{\Omega t_1}{2}}\, |+y\rangle + e^{-i\frac{\Omega t_1}{2}}\, |-y\rangle\right) \\
&= \frac{-1}{\sqrt{2\pi}} e^{i\left(ky - \frac{\hbar k^2}{2m}t_1\right)} \begin{pmatrix} \cos\left[\frac{\Omega t_1}{2}\right] \\ \text{-sin}\left[\frac{\Omega t_1}{2}\right] \end{pmatrix}\ ,
\end{aligned}
\tag{4.2}
$$

where $\chi_1(t_1, \Omega)$ indicates the outcome of the spinor function after the rotation. For 2π the polarisation vector Eq. (3.18) becomes

$$
\mathbf{P}_1(\alpha_1 = 2\,\pi) = \begin{pmatrix} -sin[\Omega t_1] \\ 0 \\ cos[\Omega t_1] \end{pmatrix}\ . \tag{4.3}
$$

The decisive difference to a static spin flipper ($\Omega = 0$) is that the polarization vector is not reverting exactly back to its initial direction, but is positioned somewhere in the xz-plane depending on the frequency of the rotating magnetic field. This is the observational consequence that was predicted in [35] for a neutron interferometer experiment.

Scanning coil

After the AC spin rotator, the neutrons re-enter the area of the guide field and start to precess around the z-axis. The intensity at the detector corresponds to the projection of the polarization vector onto the z-axis, so the guiding field leaves the intensity unchanged. Instead of recording only a single point for each frequency, it is possible to get a full oscillographic picture per frequency by employing a DC-flipper after the AC-coil. This scanning process incorporates another parameter, that can be varied to generate a periodic intensity modulation.
If the distance between the AC-coil and the scanning coil is chosen, so that the 'amount' of precession inside the guide field, i.e. the rotation angle α_2, equals $(2m+1)\,\frac{\pi}{2}, m \in \mathbb{N}$ then the polarisation vector of the neutron will turn into the yz-plane

$$\chi_2(t_2) = e^{-i\left(\frac{\hbar k^2}{2m}t_2\right)}\, e^{-i\frac{\alpha_2}{2}\sigma_z}\, \chi_1(t_1,\Omega)\Big|_{\alpha_2=(2m+1)\frac{\pi}{2}} \tag{4.4}$$

$$\mathbf{P}_2\left(\alpha_1 = 2\pi, \alpha_2 = (2m+1)\,\frac{\pi}{2}\right) = \begin{pmatrix} 0 \\ -\sin[\Omega t_1] \\ \cos[\Omega t_1] \end{pmatrix} . \tag{4.5}$$

Afterwards the neutron enters the scanning coil where a magnetic field B_{3x} is varied to finally give an oscillating signal, with

$$\chi_3(t_3) = e^{-i\left(\frac{\hbar k^2}{2m}t_3\right)}\, e^{-i\frac{\alpha_3}{2}\sigma_x}\, \chi_2(t_2) \tag{4.6}$$

and for the final wave-function ψ_f

$$\psi_f = \frac{1}{\sqrt{2\pi}} e^{i\left(ky-\frac{\hbar k^2}{2m}T\right)}\, e^{-i\frac{\alpha_3}{2}\sigma_x}\, e^{-i(2m+1)\frac{\pi}{4}\sigma_z}\, \frac{1}{\sqrt{2}}\left(e^{i\frac{\Omega t_1}{2}}\,|{+y}\rangle + e^{-i\frac{\Omega t_1}{2}}\,|{-y}\rangle\right) , \tag{4.7}$$

where $T = t_1 + t_2 + t_3$ and $\alpha_3 = \gamma t_3 B_{3x}$.
Calculating the expectation value in this state $\psi_f(y, T, \Omega)$ the final polarization looks in the following direction

$$\mathbf{P}_f = \begin{pmatrix} 0 \\ -\sin[\alpha_3 + \Omega t_1] \\ \cos[\alpha_3 + \Omega t_1] \end{pmatrix} . \tag{4.8}$$

This result in comparison with the polarization vector given by Eq. (4.3) shows that the phase shift from the spin-rotation coupling has been preserved and differs only by a variable parameter α_3, controlled via the static magnetic field B_{3x}. The analyzer (i.e. the second supermirror) at the end of the set-up post-selects only the $|{+z}\rangle$ spin states, which leads to an intensity $I = |\langle +z|\psi_f\rangle|^2$. Thus the measurement at the detector will show the following sinusoidal form

$$I(\Omega, \alpha_3) = \cos\left[\frac{\alpha_3 + \Omega t_1}{2}\right]^2 . \tag{4.9}$$

This outcome indicates the expected results of the actual experiment. For each frequency of the AC spin rotator an oscillographic signal is going to be recorded with a constant phase shift. The shift of the intensity maximum between $-\pi$ and π is given by

$$\alpha_3 = -\Omega t_1 . \tag{4.10}$$

It is important to check what consequences occur, if the rotation angle α_1 does not correspond to a 2π rotation. The intensity for the same set-up with a general rotation angle α_1 is

$$\begin{aligned} I(\Omega, \alpha_1, \alpha_3) &= \frac{1}{2}\left(1 + \cos[\alpha_1]\,\cos[\alpha_3 + \Omega t] + \frac{\Omega}{\gamma B_{eff}}\sin[\alpha_1]\,\sin[\alpha_3 + \Omega t]\right) \\ &= \frac{1}{2}\left(1 + \cos[\alpha_1]\,\cos[\alpha_3 + \Omega t] + \frac{\sin[\alpha_1]\,\sin[\alpha_3 + \Omega t]}{\sqrt{\left(\frac{B_0\gamma}{\Omega}\right)^2 + 1}}\right) . \end{aligned} \tag{4.11}$$

This implies for $\alpha_1 \neq 2n\pi$ that the intensity maximum does not only shift, but also decrease in amplitude, i.e. a decrease of the contrast. Physically this corresponds to the general case given by (3.17), where the polarization vector has components in all axes.

4.3 Adjustments

The following explanations will describe the various actions that have been undertaken in the experimental process.

The first step was to adjust the Helmholtz coils, for which all unnecessary components between the source and the detector were removed. Two Co-Ti supermirrors were used. The first one guided and polarized the neutrons that came from the reactor, while the second one, which was installed at the other end of the Helmholtz coil, was used as an analyzer that only reflected one of the spin states to the detector. To remove higher order harmonics the incident angle between the second supermirror and the center of the neutrons' flight path was slightly detuned. A Cd-diaphragm with an opening of 6 mm $\times$ 15 mm served as a collimator for the neutron beam. After aligning the height and the distance of the pair of *Helmholtz* coils the degree of polarization in this 'empty polarimeter set-up' was brought to a maximal value of roughly 99% for B_{gf} =10 G.

4.3.1 Small coil

In the next step the coils had to be inserted and adjusted. By default, the coils in use are the small ones as shown on the right side of Fig. 3.4. Because of their compact size they are insusceptible to most inhomogeneities of the exterior magnetic field and can be easily aligned, for which a good example is depicted in Fig. 4.3. Typical maximal intensity was 0.38 n/sec. The sinusoidal intensity modulation is characterized by the contrast C, defined as:

$$C = \left| \frac{I_{max} - I_{min}}{I_{max} + I_{min}} \right| . \tag{4.12}$$

The graph Fig. 4.3 exhibits a reasonable curve progression of a typical DC-flipper. Zero current implies zero magnetic field in the coil, so that the spin passes through the coil unchanged. For ($\pm$) $\approx$1182 mA a ($\pm$) π spin flip of the neutrons is induced, which are thereafter 'sorted out' from the analyzer, i.e. the second supermirror. A misalignment of the coil would appear as a phase shift and cause an asymmetry of the intensity at the minima.

4.3.2 Big coil

The disadvantage of a small coil in the case of a rotating field can be clearly seen by restating the relation (3.12) in the form

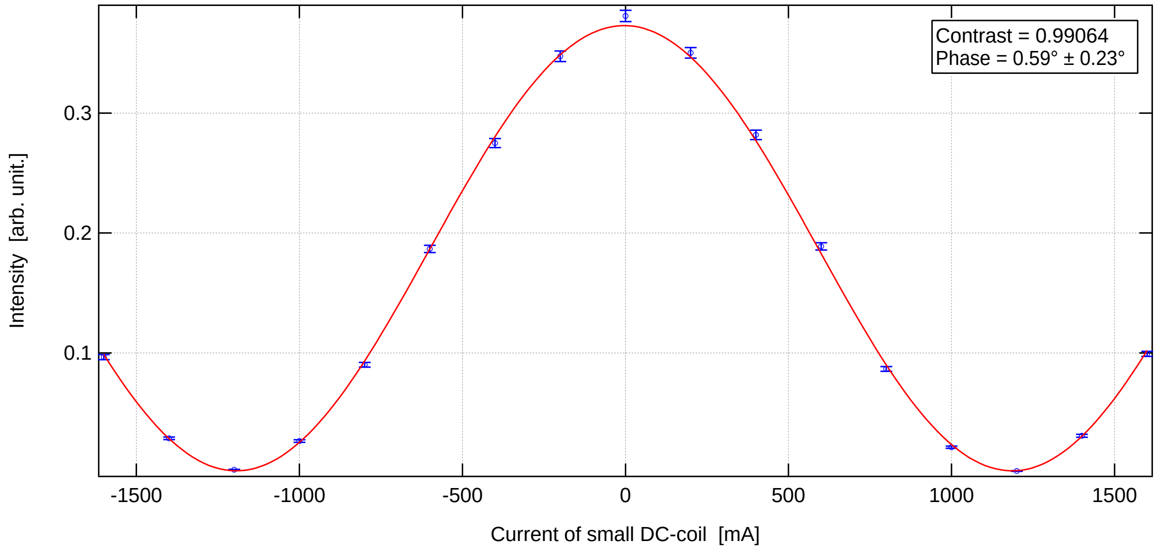

Figure 4.3: Almost perfectly aligned coil with a high contrast of rougly 99% and a phase shift less then 1°.

$$\Omega = 2\pi\nu = \sqrt{\left(\frac{\alpha_1}{t}\right)^2 - {B_0}^2\gamma^2} = \sqrt{\left(\frac{2\pi\, v_n}{l}\right)^2 - {B_0}^2\gamma^2}\,. \tag{4.13}$$

For a 2π rotation and a mean abode time $t = l/v_n$ of the neutrons, the frequency Ω is determined by the length of the coil. As experience has shown, high frequencies, circa at 50 kHz and above for instance, lead to undesired problems, mostly caused by parasitic effects in the coil, which make it hard to generate a homogeneous, uniformly rotating magnetic field. Furthermore, a *resonant circuit* would have to be build for each frequency to minimize the electrical impedance and enable enough current to pass the coil.

To avoid this issues the length of the coil was increased to $l = 20$ cm (see left photo in Fig. 3.4). The frequency-dependence $\Omega(B_0)$ of the magnetic field's amplitude B_0, required to accomplish a 2π rotation, is plotted in Fig. 4.4 for a neutron velocity of $v_n \approx 2000$ m/s. The increase of length of the coil has reduced the necessary frequencies to a maximum of 10 kHz, which is moderate for operation. The stronger the magnetic field, respectively the current in the coil, the less angular velocity is needed with a minimum at approximately B_0 (0 kHz) $= 3.4$ G.

Before the appliance of the coil as an AC spin rotator, the alignment had to be made, which needed to be performed in DC mode. The enlargement of the coil however brought

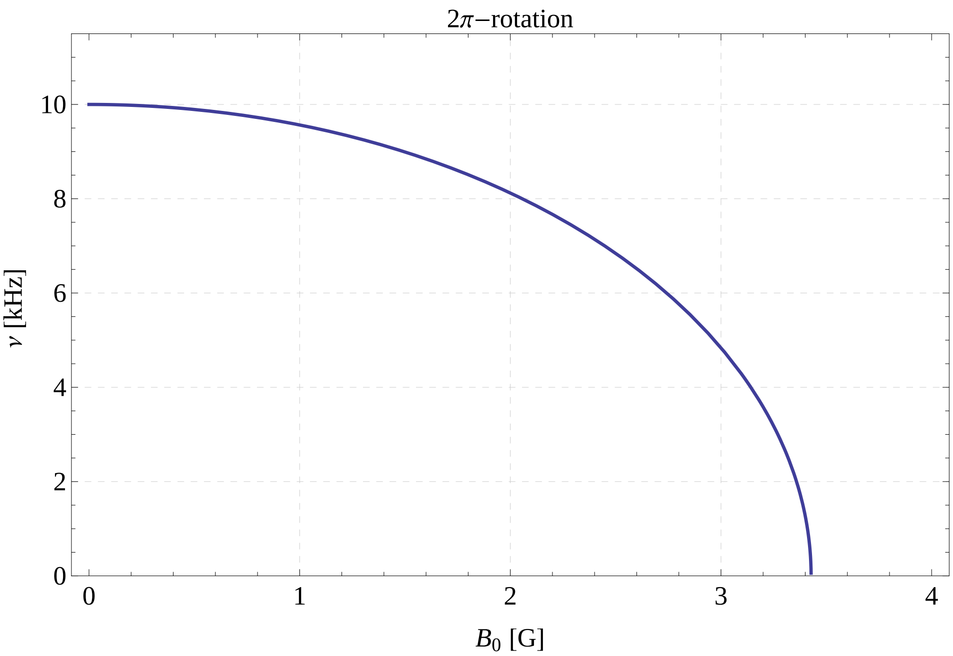

Figure 4.4: Only values on the arc correspond to a 2π flip for a coil of 20 cm lenght and a neutron velocity of $v_n \approx 2000$ m/s.

along two major difficulties. Firstly, increased susceptibility to misalignments and secondly, problems in obtaining non-adiabatic conditions. The following approaches were made to resolve these issues.
To correctly align the big coil in z-direction a '(de)acceleration' test was performed in the middle of the polarimeter. The principle of this test is depicted in Fig. 4.5. Neutrons with up-spin are flipped into the xy plane and precess about the magnetic field of the big coil, which is modulated to generate a periodic signal. If the the big coil is misaligned the contrast will decrease, contrariwise if the directions of the guide field and the magnetic field coincide the spin can be fully flipped back to the z-axis for the appropriate field configuration.
Figure 4.6 shows the result of such a measurement, where three sinusoidal fits have been made to determine the contrasts. The direction of the magnetic field in the big coil was set to compensate the exterior guide field. According to the graph the contrast increases for higher currents, i.e. less field in the coil, hence lower *Larmor* frequency. This fact explains the term deacceleration test. Of course the same experiment could have been made for the case of both fields adding up.
As a side note, it can be seen that the contrast reaches 'only' a value of rougly 96%.

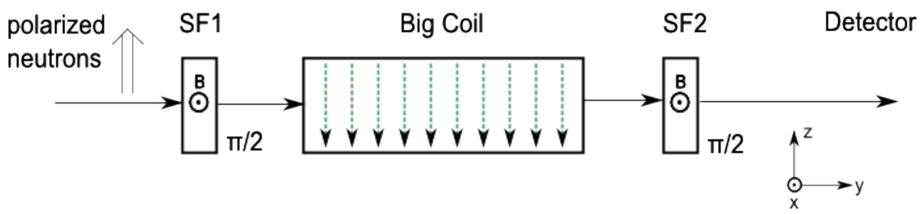

Figure 4.5: Initially $\chi(0) = |+z\rangle$ spins are flipped by $\frac{\pi}{2}$ in the first small coil. The second $\frac{\pi}{2}$ flipper will only be able to flip the neutrons back into the z-direction, when the directions of the guide field and the magnetic field of the big coil coincide.

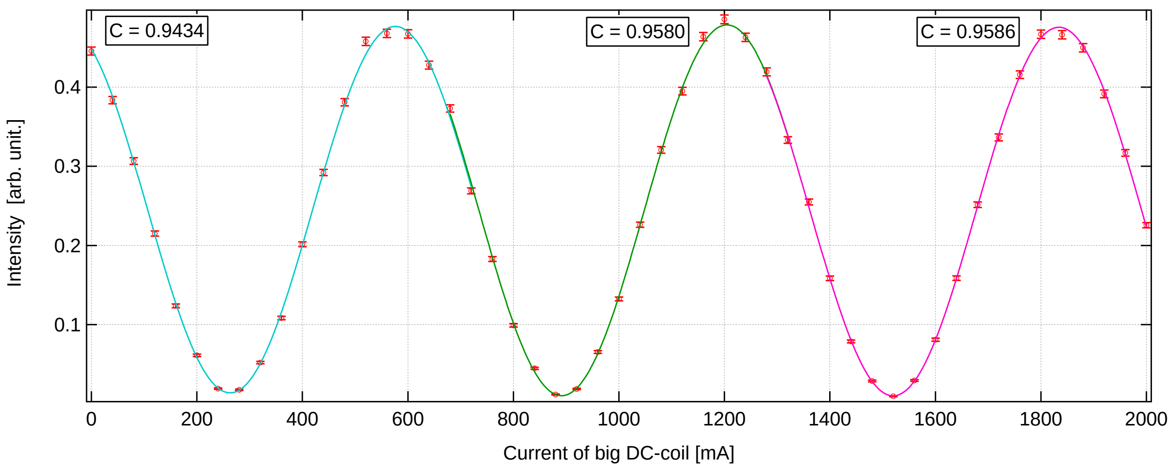

Figure 4.6: Oscillations of the big coil in the $\frac{\pi}{2}$-$\frac{\pi}{2}$ set-up in each region.

This is primarily caused by a slight loss of neutrons at each coil, due to absorption in the copper wires or depolarization due to large rotation angle, which itself depends again on the wavelength (respectively velocity). It can also be noticed that the intensity changed in comparison to Fig. 4.3. The source of this are occasional changes of the Cd-diaphragm opening.

Switching to the x-field in the big coil was way more troublesome then the alignment in the z-direction. In a first attempt the coil was used without a compensation field. The consequences can be seen in Fig. 4.7.

The form of the curve for low currents strongly differs from a cosine, because the guide field exceeds the field in the x-direction. Since the lengthening of the coil has reduced the field strength needed to induce a π flip, no changes of the polarization can be observed in the low limit. To affirm this idea the magnitude of the guide field was reduced by one-third. The result is shown in Fig. 4.8, where it can be seen that the 'recess' of the function has gotten deeper.

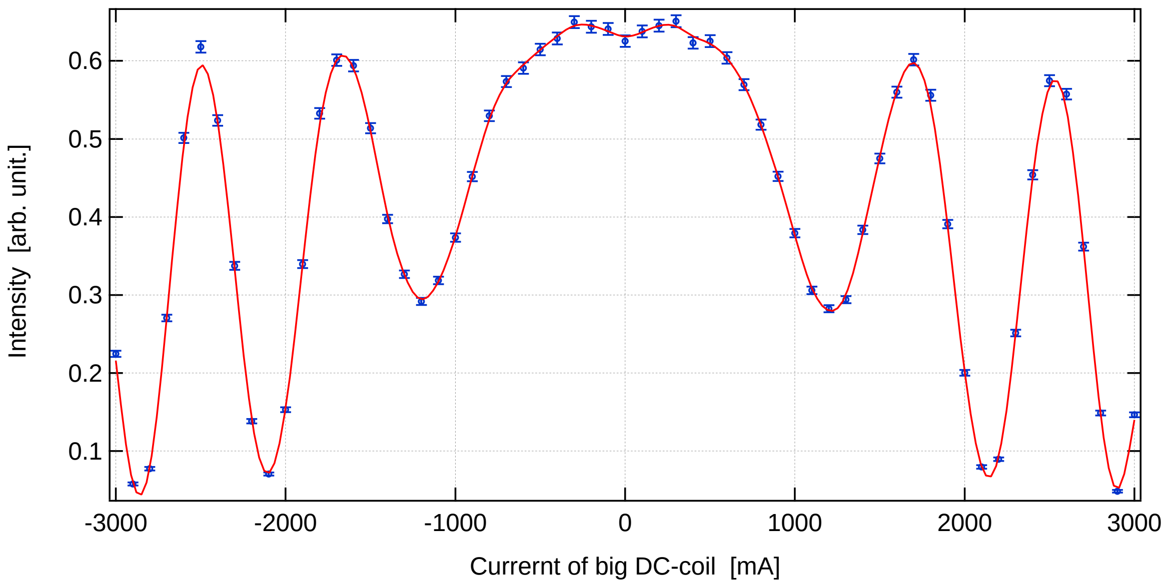

Figure 4.7: Big coil with a magnetic field in x-direction only, thus uncompensated. 'Lower order spin flips' are suppressed from the B_{gf}=15 G guide field.

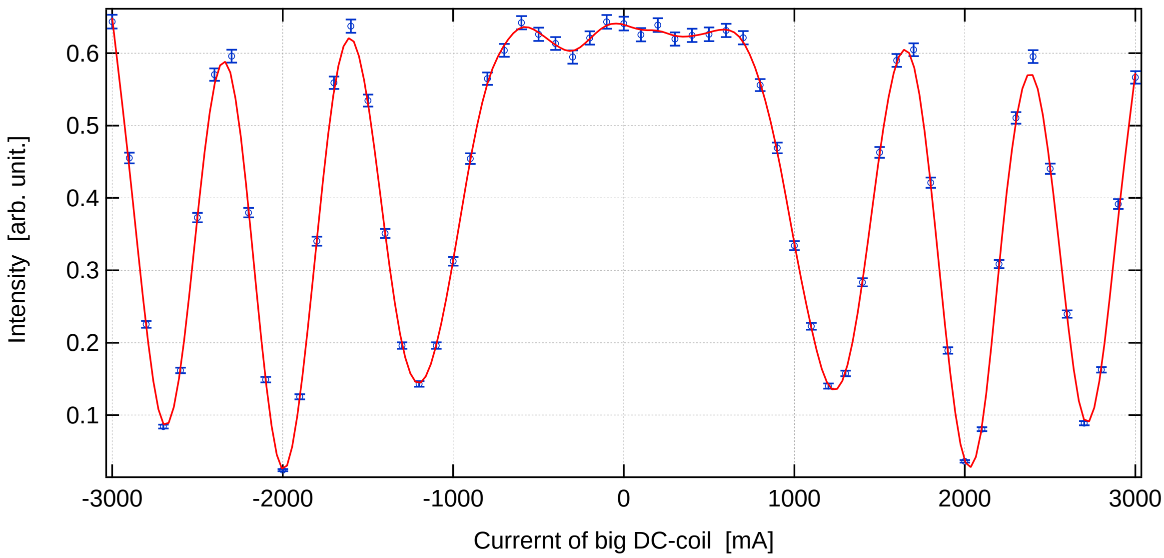

Figure 4.8: B_{gf}=10 G. The next minima started to appear after the guide field was reduced.

In the next step the compensation field was turned on. Unfortunately, this has not brought the desired result. Although the minima of the $\pm\pi$ - flip were recovered, the peaks were still at different levels. See Fig. 4.9.

After some consideration, we found that this asymmetry at higher currents stems from

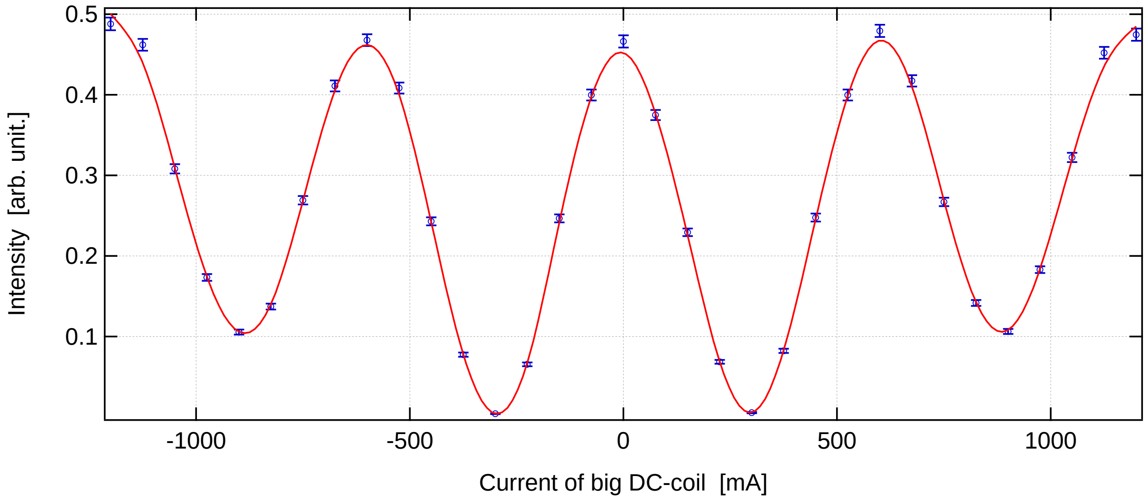

Figure 4.9: Big Coil with compensation field switched on. The higher order minimas show that the spin of the neutrons are only partially flipped.

non-adiabatic alteration of the neutron spin. In the compensated state small magnetic fields have no influence outside of the coil, but with increasing current this range expands, engulfing the vicinity with a weak magnetic field, that change the initial polarization of the neutron prior to the entry into the coil.
The first measure to get rid of this effect was to increase the guide field's magnitude, which proved to be both ineffective and disadvantageous. Instead, two additional small DC-coils were placed directly before and after the big coil, each generating an additional magnetic field in the negative z-direction. This 'sandwich' arrangement enabled to successfully operate the big coil as a standard DC-flipper and correctly align it in the polarimeter. Figure 4.10 shows the final adjustment of the big coil.

4.3.3 AC Set-up

Employing the big coil as a time-dependent sinusoidal spin rotator was only a matter of connecting the wires to a signal generator and an amplifier. To generate a compensation field, the current of the periodic signal for the z-direction had to be superposed with a DC bias current. Since the amplifier would not respond to the bias of the function generator (probably AC-coupled, so it only amplifies signals which change with time), it was set at the amplifier itself. To monitor the current signal of the conductor a current clamp was used to read the magnitude of the sinusoidal signal. The input signals and the induced

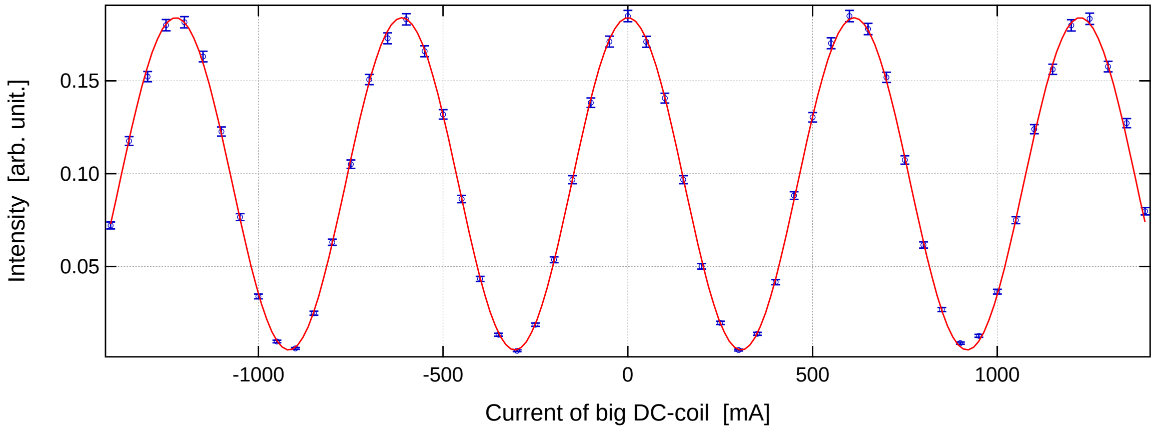

Figure 4.10: Best aligned big coil exhibits a contrast of C = 0.94549, Period = 611.89 ± 0.28 and a phase offset of $-0.71° \pm 0.21°$.

current in the current clamp were all connected and monitored on an oscilloscope. An illustration of the various connected tools is shown in Fig. 4.11

The following settings were made to generate the correct inputs. Two periodic signals with a phase shift of 90° were triggered and the bias was set at the amplifier. To induce a 2π rotation of the spin, the appropriate values of frequency and amplitude had to bee set in each coil (see Fig. 4.4). After the fixing of the frequency and setting the current of the scanning coil to the point of the expected phase shifted maximum, the amplitude was varied. According to Eq. (4.11) the maximal intensity only occurs for the appropriate amplitude. This procedure was executed for each frequency.

It should be mentioned that for increasing frequencies the amplitude did not behave as Fig. 4.4 would imply, due to the impedance of the coil. Instead of connecting the circuit with two capacitors and operate in resonance mode, the voltage was increased. A short comparison for 5 kHz showed that approximately the tenfold voltage was required because of the dissipation. For an electrical resistance of R = 1 Ω approximately 9 V at 9 kHz were needed, which corresponds to only ≈ 1 G. It can be assumed that higher frequencies will most likely have to handle with the damping by incorporating a *resonant circuit*.

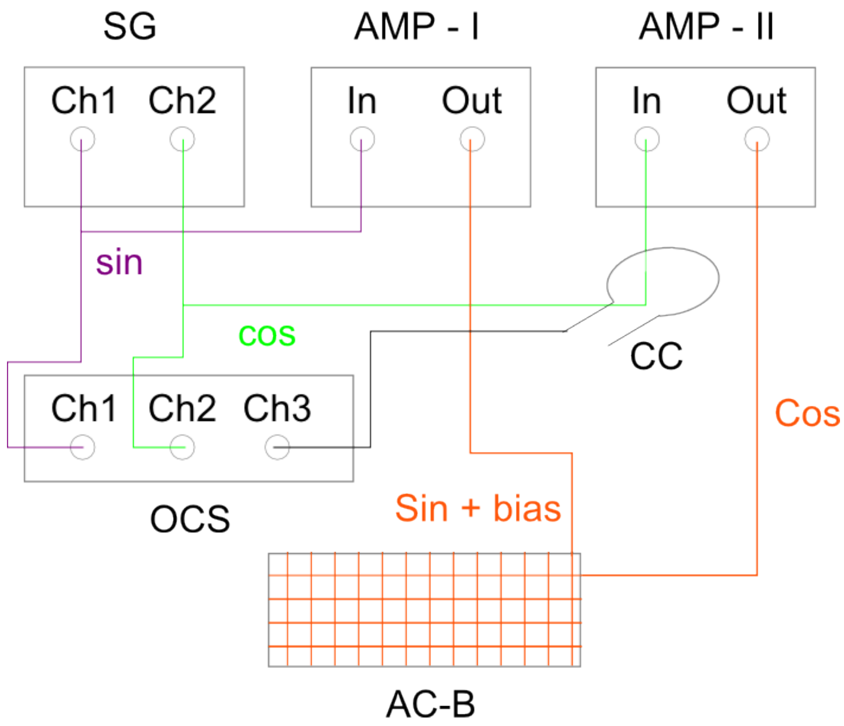

Figure 4.11: Connections applied for AC operation mode. (SG) Signal generator (Yokogawa - FG120) with two channels connected. (Amp-I) First power amplifier (EPS - TO/E7610); (Amp-II) Second power amplifier (EPS TO/E7610). (CC) Current clamp (TEKTRONIX - P6021A AC); (OSC) Oscilloscope (TEKTRONIX - TDS 2004B); (AC-B) Big AC-coil.

4.4 Measurement of the spin rotation phase shift

Before presenting the experimental results the final arrangement is shown in Fig. 4.12, which has changed slightly in comparison to Fig. 4.2, since two additional coils were added to avoid adiabatic phase shifts. Moreover the final parameters, for which all subsequent results were measured, are summarized in Tab. 4.1. All coils were aligned and the distance between the coils was set.

The frequencies and strengths of the magnetic field were adjusted for 12 different values and each of them was measured three times at least to reduce statistical errors. The corresponding amplitudes varied between 3 V and 9 V and were determined by the method described in the previous section.

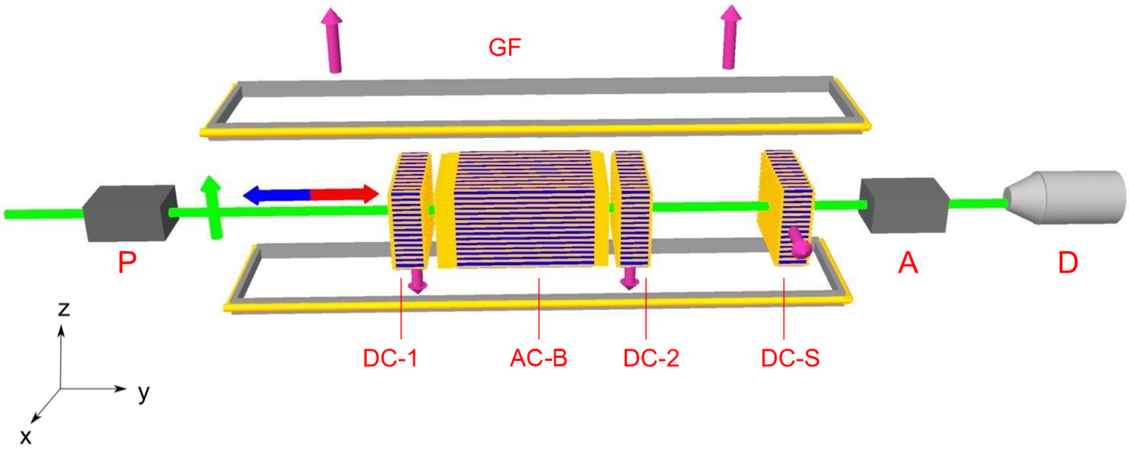

Figure 4.12: Final set-up. (P) 1st supermirror polarizer; (GF) guide field; DC-1) First additional DC-coil; (AC-B) Big AC-coil; (DC-2) Second DC-coil; (DC-S) Scanning DC-coil; (A) 2nd supermirror analyzer; (D) detector.

Quantity	Value
Aperture: B $\times$ H	6 mm $\times$ 15 mm
Guide field B_{gf}	5 G
Compensation current for the big AC-coil	948 mA
Current in the small coils	236 mA

Table 4.1: Final test parameters of the experiment.

According to Eq. (4.10) the phase shift in degrees is given by

$$\alpha_3 = -2\pi\nu\frac{l}{v_n} \cong -\frac{360[\mathrm{deg}]\, 0.2\,\mathrm{m}}{2000\,\frac{\mathrm{m}}{\mathrm{s}}}\nu = -36\left[\frac{\mathrm{deg}}{\mathrm{s}}\right]\nu[\mathrm{kHz}]\,. \tag{4.14}$$

This relation shows the advantage of the polarimeter again. Pro 1 kHz, an absolute phase shift by 36 [deg] is expected in the 20 cm coil.

For $\Omega = 0$ kHz the the big coil is only working as a DC-flipper in practice. There is no change of the polarization vector between the initial and the final state. Therefore the result equals the form in Fig. 4.3. The other frequencies are phase shifted due to the spin-rotation coupling. The results are all assembled and shown in Fig. 4.13 and Fig. 4.14. For optical aid the graphs on one site run from top to bottom.

Each of these intensity oscillations was measured for three times at least. To check the systematic reproducibility of the phase shift the oscillations of the frequency 5 kHz were measured another three times consecutively under the same conditions. The deviation between the maximum and minimum value of the phase shift for 5 kHz yielded a repeatability rate of roughly 1.14°. Apart from the statistical deviation (least square fit, confidence interval 68.3%) each standard deviation is corrected by this rate. Other sources of error, e.g. length of the coil, monochromaticity, distance between the coils, are omitted, since their contributions are assumed to be negligibly small compared with this systematic value. The final results are summarized in Tab. 4.2, which show a good agreement between the obtained values and the theoretical values.

ν [kHz]	ϕ [°]	C	$\lvert\alpha_3\rvert$ [°]
0	-0.46 ± 1.51	0.972 ± 0.002	0
1	35.43 ± 1.40	0.938 ± 0.003	36
2	71.76 ± 1.42	0.968 ± 0.003	72
2.5	88.83 ± 1.45	0.964 ± 0.002	90
3	107.88 ± 1.41	0.952 ± 0.005	108
4	143.71 ± 1.53	0.952 ± 0.012	144
5	179.64 ± 1.46	0.958 ± 0.002	180
6	215.16 ± 1.43	0.944 ± 0.015	216
7	254.27 ± 1.44	0.936 ± 0.022	252
7.5	269.78 ± 1.47	0.943 ± 0.020	270
8	289.54 ± 1.49	0.913 ± 0.026	288
9	325.59 ± 1.43	0.940 ± 0.026	324

Table 4.2: Final phase shifts and contrasts for each frequency. Predicted values on the right column.

Except for 7 kHz, 8 kHz and 9 kHz all measurements are within the error bounds of the theoretically predicted values. The frequency dependences of the phase shift and the contrast are plotted in Fig. 4.15 and Fig. 4.16 respectively. The linear dependence is in agreement with Eq. (4.14).

The contrasts of almost all measurements are over 94% on average, with a minimum for 8 kHz at 91.3 %. It is assumed that the decrease of the contrast for higher frequencies

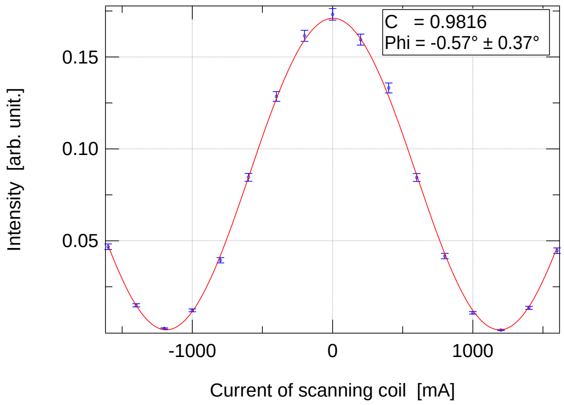

(a) 0 kHz.

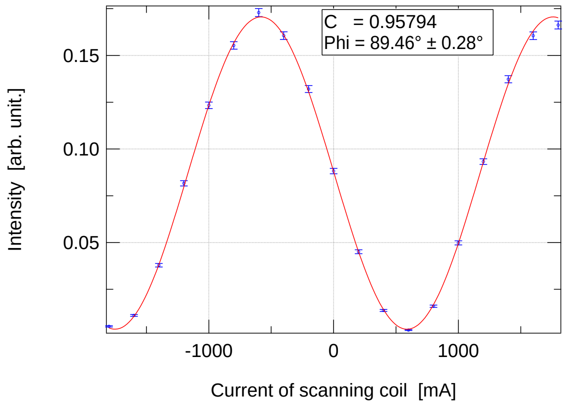

(b) 2.5 kHz.

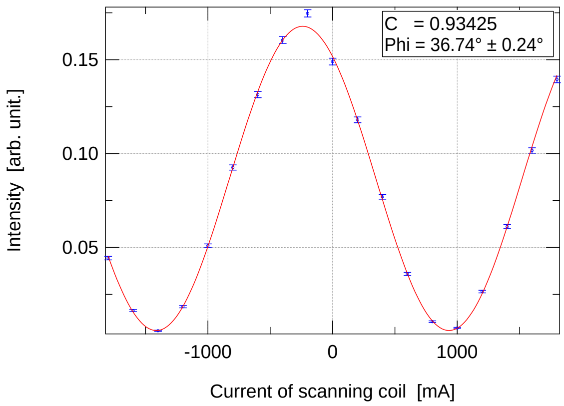

(c) 1 kHz.

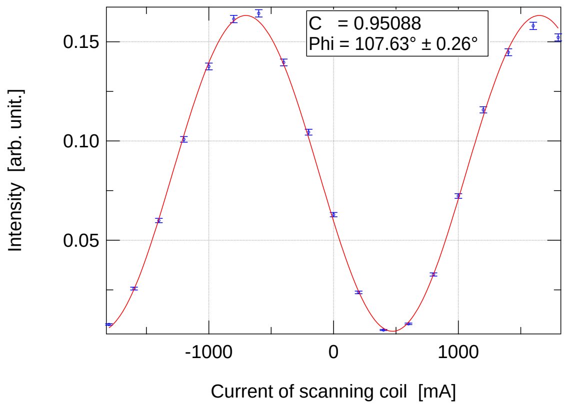

(d) 3 kHz.

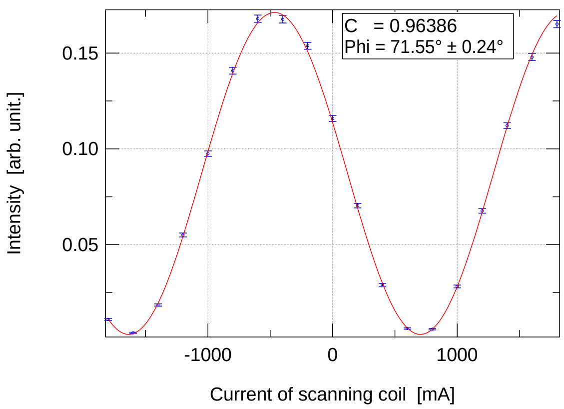

(e) 2 kHz.

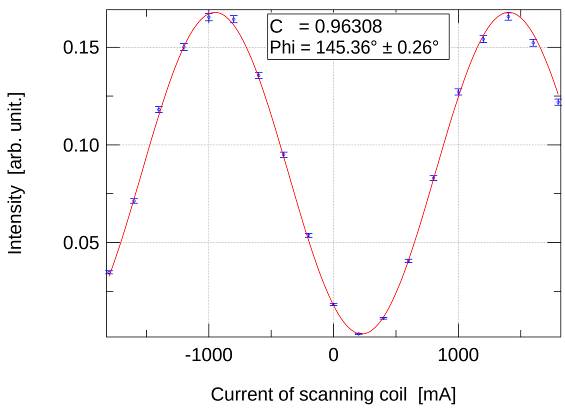

(f) 4 kHz.

Figure 4.13: Typical intensity modulations obtained by scanning the current of the DC-S. Sinusoidal modulations are shifted due to spin-rotation coupling. Contrast C and Phase shift *Phi* are also shown for each result, which run from 0 - 4 kHz.

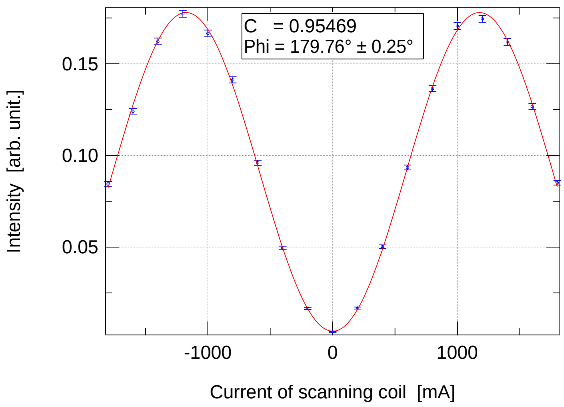

(a) 5 kHz.

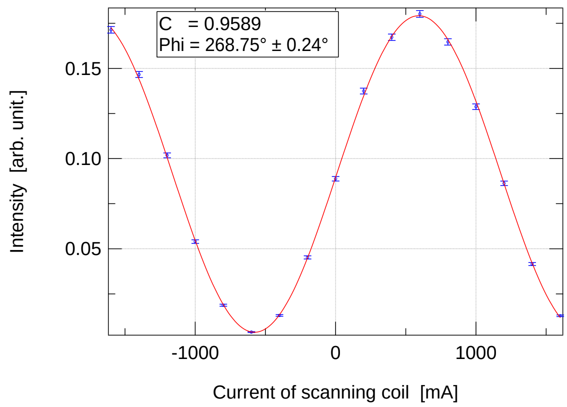

(b) 7.5 kHz.

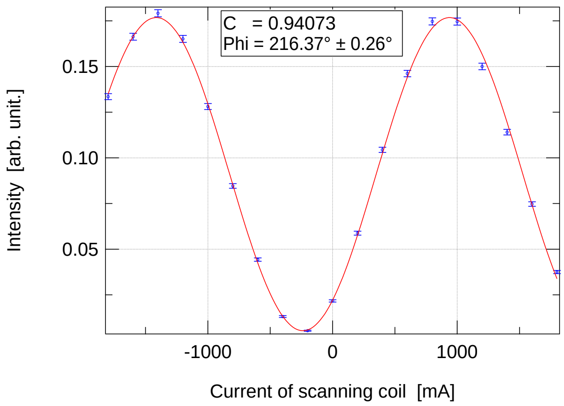

(c) 6 kHz.

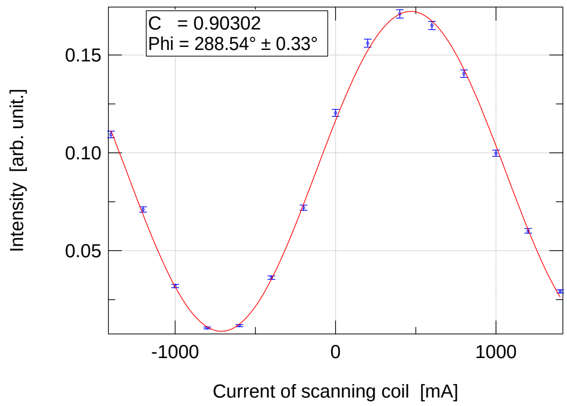

(d) 8 kHz.

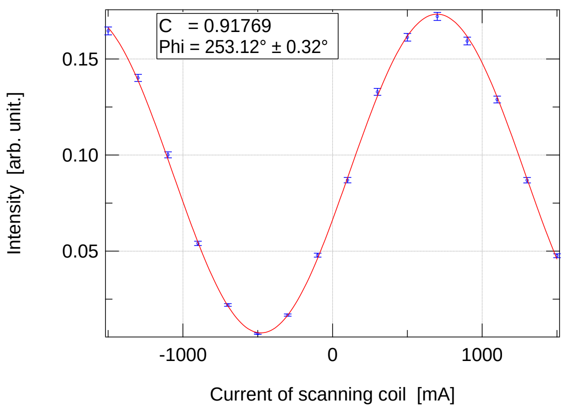

(e) 7 kHz.

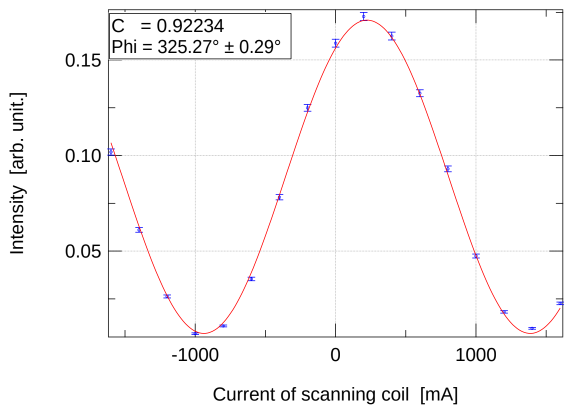

(f) 9 kHz.

Figure 4.14: Typical intensity modulations obtained by scanning the current of the DC-S. Sinusoidal modulations are shifted due to spin-rotation coupling. Contrast C and Phase shift *Phi* are also shown for each result, which run from 5 - 9 kHz.

has two sources. On the one hand, at higher impedances the resistive losses in the windings start to appear and cause inhomogeneities, on the other hand higher frequencies correspond to lower magnetic field making the coil more susceptible to the influence of exterior magnetic fields.

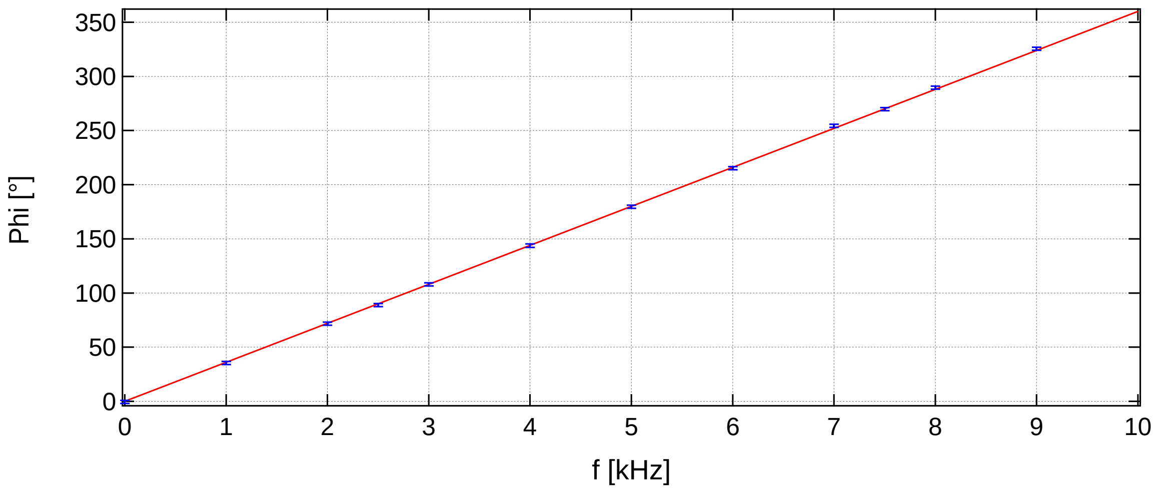

Figure 4.15: Linear phase shift. The blue points represent the measured points, while the red lines indicates the ideal value.

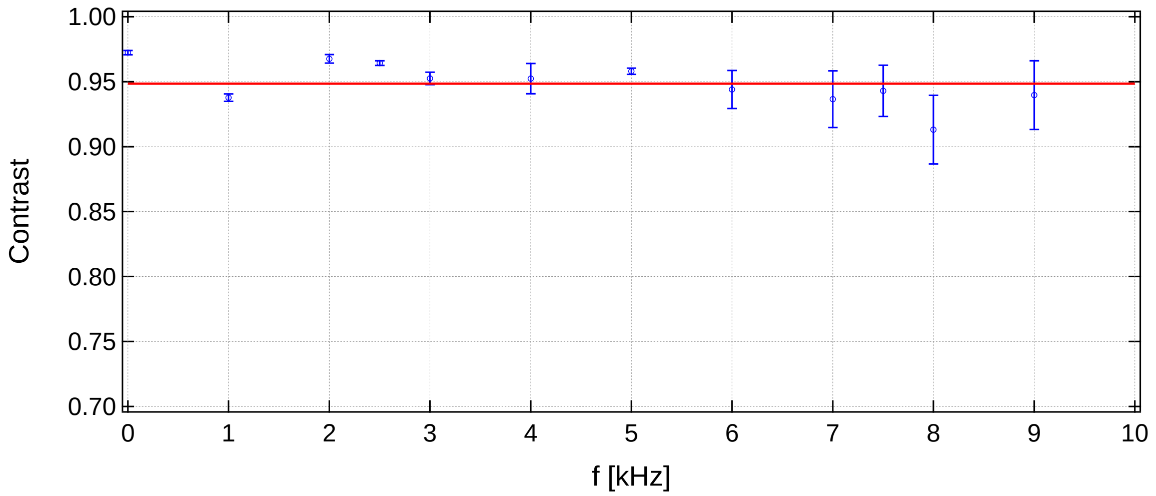

Figure 4.16: Development of the contrast for different frequencies. To guide the eye, the average value has been placed on the graph as well.

5 Conclusion

In this thesis, spin rotation coupling has been studied and confirmed by using a neutron polarimeter set-up. For the experimental optimization the dependence of the phase shift on the frequency was calculated and it was found, that the strength of the B_x field had to be adjusted following the change of frequency (see Fig. 4.4). After consideration of *a priori* results for the proposed polarimeter set-up and the potential difficulties for coils operating at high frequencies, we found a longer AC-coil to be more advantageous. For a practical dimension of the set-up, the coil's length was determined to be 20 cm.

When the experiment was carried out, the operation of the AC-coil in the experiment posed some problems at the first stage. The issue of the stray-field was solved by inserting two additional DC-coils just before and after the big AC-coil, which ensured non-adiabatic transitions of the neutrons. It should to be stressed here that this experiment has benefited from the length of the coil, which could not have been incorporated in a neutron interferometer.

The phenomenon of spin-rotation coupling has been computed in the preliminary calculations of sec. 4.2, where the original interaction $\mathbf{\Omega} \cdot \mathbf{S}$ has been substituted via the Larmor rotation, which relates the angular velocity of a magnetic dipole with the magnetic field. This way the mechanical rotation was replaced by a rotation of a magnetic field in a quadrature coil, thus $\mathbf{B}(\Omega) \cdot \hat{\boldsymbol{\sigma}}$.

The final results obtained are in good agreement with theory and the accuracy of the values is high. The deviations from most of the predicted values are within the error bound of the measurements. The average contrast has been roughly 94%, highlighting once more the significance of the neutron polarimetry.

Further polarimeter experiments are planned in near future. It is assumed that for low frequencies no B_x field adjustment is required and the same results can be obtained in the original model of the set-up. Also a realization of the proposed experiment [35] or [6] is imaginable.

In my opinion, it will be interesting to further elucidate observational consequences of accelerated frames of reference in the quantum-physical regime.

Appendix A: Interaction in a uniformly rotating magnetic field

Derivation of the analytic solution of the wave function for a neutron in a uniformly rotating magnetic field, which has been found in [36] and [37].

For a uniformly rotating magnetic field

$$\mathbf{B}(t) = \begin{pmatrix} B_0 \, cos\Omega t \\ 0 \\ B_0 \, sin\Omega t \end{pmatrix} \qquad \mathbf{B}(t) = 0 \, \text{for} \, t < 0, t > T \tag{A.1}$$

and a particle moving into the y - direction the Schrödingergleichung equation is

$$i\hbar \frac{\partial}{\partial t}\psi(y,t) = \left(-\frac{\hbar^2}{2m}\frac{\partial}{\partial y^2} - \mu \, \hat{\boldsymbol{\sigma}}\mathbf{B}(t) \right) \psi(y,t) \, . \tag{A.2}$$

Performing a separation ansatz $\psi(y,t) = \phi(y)\chi(t) \equiv \phi(y) \begin{pmatrix} \chi_1(t) \\ \chi_2(t) \end{pmatrix}$ we receive the following two differential equations

$$i\hbar \frac{1}{\chi(t)} \frac{\partial}{\partial t}\chi(t) \, + \, [\mu B_0(\hat{\sigma}_x cos(\Omega t) + \hat{\sigma}_z sin(\Omega t))] = -\frac{\hbar^2}{2m}\frac{1}{\phi(y)}\frac{\partial}{\partial y^2}\phi(y) \equiv \lambda \, . \tag{A.3}$$

The solution of the right side for a plane wave moving into the +y direction yields

$$\phi(y) = \frac{1}{\sqrt{2\pi}} e^{iky} \, , \tag{A.4}$$

with $\lambda = \frac{\hbar^2 k^2}{2m}$, whereas the differential equation of the time dependent spinor gives

$$i\hbar\frac{1}{\chi(t)}\frac{\partial}{\partial t}\chi(t) \;+\; [\mu B_0(\hat{\sigma}_x cos(\Omega t) + \hat{\sigma}_z sin(\Omega t))] = \frac{\hbar^2 k^2}{2m}\,. \tag{A.5}$$

Doing the following substitution

$$\chi(t) = \xi(t)e^{-i\frac{\hbar k^2}{2m}t} \tag{A.6}$$

transforms the last equation into a homogeneous differential equation

$$i\hbar\frac{\partial\xi(t)}{\partial t} \;+\; [\mu B_0(\hat{\sigma}_x cos(\Omega t) + \hat{\sigma}_z sin(\Omega t))]\xi(t) = 0\,. \tag{A.7}$$

To solve this equation we perform a transformation onto the rotating frame by the following unitary operation

$$\xi(t) = \hat{U}(t)\,\xi_r(t) = e^{i\frac{\Omega t}{2}\hat{\sigma}_y}\,\xi_r(t)\,. \tag{A.8}$$

Inserting this ansatz into Eq. (A.7):

$$-\frac{\hbar\Omega}{2}\hat{\sigma}_y\,e^{i\frac{\Omega t}{2}\hat{\sigma}_y}\xi_r(t) \;+\; i\hbar\,e^{i\frac{\Omega t}{2}\hat{\sigma}_y}\,\frac{\partial\xi_r(t)}{\partial t} \;+\; [\mu B_0(\hat{\sigma}_x cos(\Omega t) + \hat{\sigma}_z sin(\Omega t))]\,e^{i\frac{\Omega t}{2}\hat{\sigma}_y}\,\xi_r(t) = 0 \tag{A.9}$$

and multiplying from the left side with $\hat{U}^{-1}(t)$, finally yields

$$-\frac{\hbar\Omega}{2}\hat{\sigma}_y\,\xi_r(t) \;+\; i\hbar\,\frac{\partial\xi_r(t)}{\partial t} \;+\; \mu B_0\;\hat{\sigma}_x\,\xi_r(t) = 0\,, \tag{A.10}$$

where we used the fact that

$$e^{-i\frac{\Omega t}{2}\hat{\sigma}_y}\,[\hat{\sigma}_x cos(\Omega t) + \hat{\sigma}_z sin(\Omega t)]\,e^{i\frac{\Omega t}{2}\hat{\sigma}_y} = \hat{\sigma}_x\,. \tag{A.11}$$

Using the definition of the Larmor frequency $\omega_0 = -\frac{2\mu}{\hbar}B_0 = -\gamma B_0$ and rearranging the terms leads to the following equation

$$i\hbar\,\frac{1}{\xi_r(t)}\frac{\partial\xi_r(t)}{\partial t} \;=\; \left(\frac{\hbar\Omega}{2}\hat{\sigma}_y \;+\; \frac{\hbar\omega_0}{2}\hat{\sigma}_x\right)\,. \tag{A.12}$$

This equation can finally be integrated, giving the following solution

$$\xi_r(t) = e^{-i\left(\frac{\Omega}{2}\hat{\sigma}_y + \frac{\omega_0}{2}\hat{\sigma}_x\right)t}\, \xi_r(0) = e^{-\frac{i}{2}\boldsymbol{\alpha}\cdot\hat{\boldsymbol{\sigma}}}\, \xi_r(0)\ , \tag{A.13}$$

where $\boldsymbol{\alpha} = (\omega_0 t, \Omega t, 0)^T = \alpha(t)\,\hat{\boldsymbol{a}}$ is the rotation vector,

$$\alpha(t) = t\sqrt{{\omega_0}^2 + \Omega^2} = \gamma t \sqrt{{B_0}^2 + \left(\frac{\Omega}{\gamma}\right)^2} \equiv \gamma t B_{eff} \tag{A.14}$$

is the magnitude and $\hat{\boldsymbol{a}} = -\hat{\boldsymbol{B}}_{eff}$ the unit vector of the rotation. Undoing the previous transformation, the time evolution of the spin in this uniformly rotating frame is given by

$$\chi(t) = e^{-i\frac{\hbar k^2}{2m}t}\, e^{i\frac{\Omega t}{2}\hat{\sigma}_y}\, e^{-\frac{i}{2}\boldsymbol{\alpha}\cdot\hat{\boldsymbol{\sigma}}}\, \chi(0) \tag{A.15}$$

and finally the wave-function is given by

$$\psi(y,t) = \frac{1}{\sqrt{2\pi}} e^{i\left(ky - \frac{\hbar k^2}{2m}t\right)}\, e^{i\frac{\Omega t}{2}\hat{\sigma}_y}\, e^{-\frac{i}{2}\boldsymbol{\alpha}\cdot\hat{\boldsymbol{\sigma}}}\, \chi(0)\,. \tag{A.16}$$

Using the identity $e^{-\frac{i}{2}\boldsymbol{\alpha}\cdot\hat{\boldsymbol{\sigma}}} = \left[\mathbb{1}\, cos\left(\frac{a(t)}{2}\right) - i\,\hat{\boldsymbol{\sigma}}\,\hat{\boldsymbol{a}}\, sin\left(\frac{a(t)}{2}\right)\right]$ the matrix representation of the wave-function can be written as

$$\begin{aligned}\psi(y,t) = \frac{1}{\sqrt{2\pi}} e^{i\left(ky - \frac{\hbar k^2}{2m}t\right)} &\begin{pmatrix} \cos\left[\frac{\Omega t}{2}\right] & \sin\left[\frac{\Omega t}{2}\right] \\ -\sin\left[\frac{\Omega t}{2}\right] & \cos\left[\frac{\Omega t}{2}\right] \end{pmatrix} \times \\ \times &\begin{pmatrix} \cos\left[\frac{\alpha}{2}\right] & -\frac{(iB_0\gamma + \Omega)\sin\left[\frac{\alpha}{2}\right]}{B_{eff}\gamma} \\ \frac{(-iB_0\gamma + \Omega)\sin\left[\frac{\alpha}{2}\right]}{B_{eff}\gamma} & \cos\left[\frac{\alpha}{2}\right] \end{pmatrix} \chi(0)\,.\end{aligned} \tag{A.17}$$

The consequences of this result are analyzed for an initial spin state of $\chi(0) = |+z\rangle = \frac{1}{2}\left(|+y\rangle + |-y\rangle\right)$ in sec. 3.3 and 4.2.

Bibliography

[1] B. Mashhoon, Neutron interferometry in a rotating frame of reference, *Phys. Rev. Lett.* **61**, 2639 (1988).

[2] S. A. Werner, J. L. Staudenmann and R. Colella, Effect of Earth's Rotation on the Quantum Mechanical Phase of the Neutron, *Phys. Rev. Lett.* **42**, 1103 (1979).

[3] B. J. Venema, P. K. Majumder, S. K. Lamoreaux, B. R. Heckel and E. N. Fortson, Search for a coupling of the Earth's gravitational field to nuclear spins in atomic mercury, *Phys. Rev. Lett.* **68**, 135 (1992).

[4] G. Badurek, H. Rauch and D. Tuppinger, Neutron interferometric double-resonance experiment, *Phys. Rev. A* **34**, 2600 (1986).

[5] N. Ashby, Relativity in the Global Positioning System, *Living Reviews in Relativity* **6** (2003).

[6] B. Mashhoon and H. Kaiser, Inertia of intrinsic spin, *Physica B* **385-386**, 1381 (2006).

[7] C. Tully, *Elementary Particle Physics in a Nutshell* In a Nutshell (Princeton University Press, 2011).

[8] A. Wachter, *Relativistic Quantum Mechanics* Theoretical and mathematical physics (Springer, 2010).

[9] T. C. Chapman and D. J. Leiter, On the generally covariant Dirac equation, *Am. J. Phys.* **44**, 858 (1976).

[10] L. Parker and D. Toms, *Quantum Field Theory in Curved Spacetime: Quantized Fields and Gravity* Cambridge Monographs on Mathematical Physics (Cambridge University Press, 2009).

[11] J. Yepez, Einstein's vierbein field theory of curved space, *arXiv:1106.2037v1 e-prints* (2011).

[12] S. M. Carroll, Lecture Notes on General Relativity, *arXiv:gr-qc/9712019 General Relativity and Quantum Cosmology e-prints* (1997).

[13] C. Misner, K. Thorne and J. Wheeler, *Gravitation* Number pt. 3 in Gravitation (W. H. Freeman, 1973).

[14] R. Sexl and H. Urbantke, *Gravitation und Kosmologie: Eine Einführung in die Allgemeine Relativitätstheorie* Spektrum-Lehrbuch (Spektrum Akademischer Verlag, 2008).

[15] W. Baylis, *Clifford (Geometric) Algebras: With Applications in Physics, Mathematics, and Engineering* (Birkhäuser Boston, 1996).

[16] L. Ryder, Spin-rotation coupling and Fermi Walker transport, *General Relativity and Gravitation* **40**, 1111 (2008).

[17] F. W. Hehl and W.-T. Ni, Inertial effects of a Dirac particle, *Phys. Rev. D* **42**, 2045 (1990).

[18] T. Padmanabhan, *Gravitation: Foundations and Frontiers* Gravitation: Foundations and Frontiers (Cambridge University Press, 2010).

[19] L. L. Foldy and S. A. Wouthuysen, On the Dirac Theory of Spin 1/2 Particles and Its Non-Relativistic Limit, *Phys. Rev.* **78**, 29 (1950).

[20] L. Ryder, Relativistic treatment of inertial spin effects, *J. Phys. A* **31**, 2465 (1998).

[21] J. Anandan and C. R. Hagen, Neutron acceleration in uniform electromagnetic fields, *Phys. Rev. A* **50**, 2860 (1994).

[22] T. Habersohn, *Erste experimentelle Versuche zur magnetischen Spintomographie mit Neutronen* (Diplomarbeit TU Wien, 2006).

[23] The TRIGA Mark-II Reactor, `http://ati.tuwien.ac.at/reactor/EN/`.

[24] H. Böck, Y. Hasegawa, E. Jericha, G. Steinhauser and M. Villa, The Past and the Future of the TRIGA Reactor in Vienna, *J. Energ. Power. Eng.* **7**, 654 (2013).

[25] G. Knoll, *Radiation detection and measurement* (Wiley, 1989).

[26] W. Stacey, *Nuclear Reactor Physics* (John Wiley & Sons, 2007).

[27] L. Dobrzyński, K. Blinowski and M. Cooper, *Neutrons and Solid State Physics* Ellis Horwood Series in Neuroscience (Ellis Horwood, 1994).

[28] C.-S. Schmitzer, *A neutron polarimetric test of Leggetts contextual model of quantum mechanics* (Diplomarbeit TU Wien, 2009).

[29] H. Rauch and S. Werner, *Neutron Interferometry: Lessons in Experimental Quantum Mechanics* Oxford in Asia. Historical Reprints (Clarendon Press, 2000).

[30] V. Sears, *Neutron optics: an introduction to the theory of neutron optical phenomena and their applications* Oxford series on neutron scattering in condensed matter (Oxford University Press, 1989).

[31] S. Sponar, *Multi-entanglement in neutron interferometric and polarimetric experiments* (Dissertation TU Wien, 2011).

[32] A. Wagh, G. Badurek, V. Rakhecha, R. Buchelt and A. Schricker, Neutron polarimetric separation of geometric and dynamical phases, *Phys. Lett. A* **268**, 209 (2000).

[33] A. G. Wagh, V. C. Rakhecha, J. Summhammer, G. Badurek, H. Weinfurter, B. E. Allman, H. Kaiser, K. Hamacher, D. L. Jacobson and S. A. Werner, Experimental Separation of Geometric and Dynamical Phases Using Neutron Interferometry, *Phys. Rev. Lett.* **78**, 755 (1997).

[34] Y. Hasegawa and G. Badurek, Noncommuting spinor rotation due to balanced geometrical and dynamical phases, *Phys. Rev. A* **59**, 4614 (1999).

[35] B. Mashhoon, R. Neutze, M. Hannam and G. E. Stedman, Observable frequency shifts via spin-rotation coupling, *Phys. Lett. A* **249**, 161 (1998).

[36] G. Badurek, *Physik polarisierter Neutronen* (Habilitationsschrift TU Wien, 1982).

[37] H. Weinfurter and G. Badurek, Measurement of Berry's phase for noncyclic evolution, *Phys. Rev. Lett.* **64**, 1318 (1990).